OUKA
The University of Osaka
Institutional Knowledge Archive

Title	Construction of an Unconventional CO2/HCOOH Cycle Based on Pentanuclear Metal Complexes
Author(s)	赤井, 拓哉
Citation	大阪大学, 2023, 博士論文
Version Type	VoR
URL	https://doi.org/10.18910/92860
rights	
Note	

The University of Osaka Institutional Knowledge Archive : OUKA

https://ir.library.osaka-u.ac.jp/

The University of Osaka

博士学位論文

Construction of an Unconventional CO_2/HCOOH Cycle Based on Pentanuclear Metal Complexes

赤井　拓哉

2023 年　2 月

大阪大学大学院工学研究科

Table of Contents

General Introduction

CO_2 utilization

The rapid increase in global energy demand caused by the rising world population and economic development has drastically accelerated the use of fossil fuels. Uncontrolled combustion of these fuels has resulted in the rapid depletion of fossil fuels and emission of large amount of greenhouse gasses such as carbon dioxide (CO_2) which causes global warming. To solve these issues, effective utilization of earth-abundant CO_2 is extremely important. In this context, the development of catalysts that can convert CO_2 into chemical feedstocks and fuels has attracted much attentions.[1-4] As shown in Figure 1, CO_2 can be converted into various kinds of chemicals such as carbon monoxide (CO) and formic acid (HCOOH) via multi-electron reduction process. Among the products of CO_2 reduction reactions, CO is a useful resource for the production of various hydrocarbons via the Fischer-Tropsch process[5,6] and C1 source for organic synthesis.[7,8] HCOOH is considered a promising hydrogen carrier and clean alternative to conventional fossil fuels. This is because hydrogen gas (H_2) is released via the dehydrogenation reaction of HCOOH. For the efficient utilization of CO_2, efficient catalysts for the production of CO (Figure 1b, (i)) and HCOOH (Figure 1b, (ii)) from CO_2 and the dehydrogenation of HCOOH (Figure 1b, (iii)) are strongly demanded. In the following sections, the details on these reactions will be described.

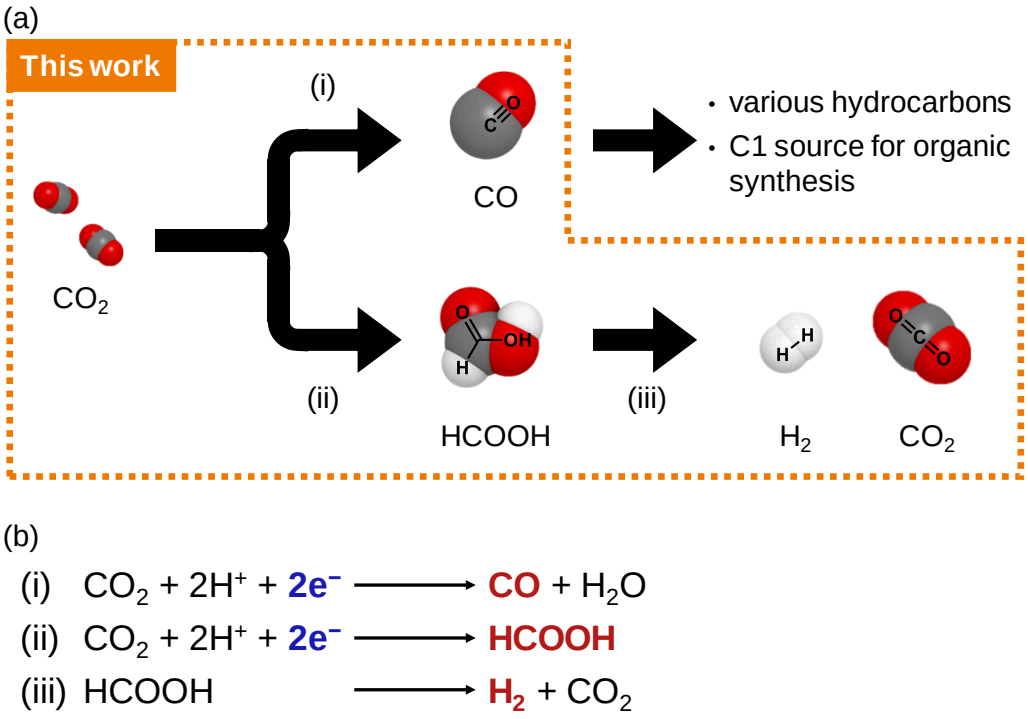

Figure 1. (a) Reactions for CO_2 utilization. (b) Reaction schemes of the CO_2 reduction (i and ii) and the HCOOH dehydrogenation (iii).

Metal-complex-based catalysts for CO_2 reduction

As mentioned in the previous section, the development of catalysts for two-electron reduction of CO_2, which yields CO ($CO_2 + 2H^+ + 2e^- \rightarrow CO + H_2O$) and HCOOH ($CO_2 + 2H^+ + 2e^- \rightarrow HCOOH$), is highly desired in recent years. Thus far, various kinds of metal-complex-based catalysts for two-electron reduction of CO_2 have been developed. CO_2 reduction mediated by metal complexes is generally initiated by the reduction of a catalyst. There are a couple of ways to supply electrons to the catalyst; (1) electrochemical and (2) photochemical methods.

In the electrochemical system, electrons are injected directly into the catalysts from the working electrode and form active species for CO_2 reduction. The injected speeds of the electrons are generally fast and the potentials applied to the electrode can be controlled. Although electrochemical CO_2 reduction is an intriguing reaction, the photochemical CO_2 reduction is preferable for the efficient utilization of renewable energy.

Most of the reported photocatalytic systems for CO_2 reduction using metal complexes consist of a photosensitizer (PS) and a catalyst (Cat). In these systems, the reduced catalytic species are generated by accepting electrons from PSs. In principle, the excitation of a PS with a single photon can induce only one-electron transfer. Thus, another electron source, such as another PS is required for the CO_2 reduction. Therefore, Cat need to accept the electron from the PS, storage two electrons, and introduce the stored electrons into CO_2 in photochemical CO_2 reduction reactions. Due to the fact that the second electron injection in photochemical process should be much slower compared to the electrochemical system, the catalyst with high electron-storage ability is required for photochemical CO_2 reduction.

Table 1 summarizes the representative examples of metal-complex-based catalysts for electro- and photochemical CO_2 reduction.[9-46] The first example of a metal-complex-based for CO_2 reduction was rhenium-based mononuclear complex, $Re(bpy)(CO)_3(X)$ (X = Cl or Br, Table 1(i)), developed by Lehn *et al.*, which drives photochemical CO_2 reduction.[9] Soon after this discovery, Tanaka *et al.*, reported the electrochemical CO_2 reduction mediated by a mononuclear ruthenium complex, $[Ru(bpy)_2(CO)_2]^{2+}$.[11] Since then, various kinds of mononuclear complexes including noble metal ions such as rhenium and ruthenium have extensively studied as catalysts for electro- and photochemical CO_2 reduction.[10,12-19] Although these catalysts are efficient, there is considerably interest in the use of cheap and abundant first-row transition metals (e.g., Mn, Fe, Co, Ni, Cu) as a substitute for noble metal-based catalysts in CO_2 reduction studies (Table 1(ii)). A remarkable example of such catalysts is iron-porphyrin complexes, of which catalytic activity was firstly revealed by Savéant *et al*.[20] The catalytic activity

of iron-porphyrin derivatives has extensively been studied both for electro-[21-24] and photo-chemical[25-28] CO_2 reduction. More recently, the catalytic activity of first-row transition metal complexes bearing a multidentate ligand is also studied.[29-34]

Another important class of compounds dinuclear metal complexes (Table 1(iii)). Dinuclear metal porphyrin complexes of Fe or Co have been reported as electrocatalysts for CO_2 reduction.[35-41] Several dinuclear metal complexes of Co or Ni work as catalysts for photochemical CO_2 reduction.[42,43] Lu and co-workers reported that a dinuclear heterometallic complex composed of Co and Zn works as an efficient photocatalyst for CO_2 reduction.[44] This dinuclear Co-Zn molecular scaffold plays an important role in C-O bond cleavage. Although reported copper-based molecular catalysts are limited, these molecular catalysts are mainly dinuclear complexes and electrochemically reduce CO_2 to CO or oxalate.[45] These reports indicate that dinuclear metal complexes work as efficient catalysts for electro- and photochemical CO_2 reduction.

Although many kinds of metal-complex-based catalysts for CO_2 reduction have been reported, the development of a catalysts with higher performance is still desired.

Table 1. Molecular metal-based catalysts for electro- and photochemical CO_2 reduction.

(i) Noble metal complexes

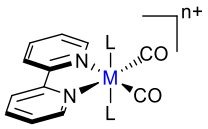

M = Ru, Re

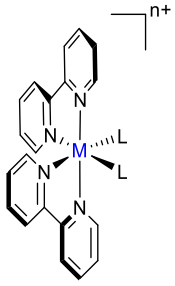

M = Ru, Rh

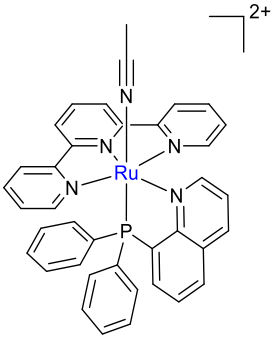

(ii) Non-noble metal complexes

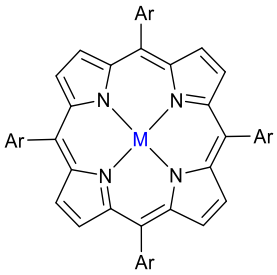

M = Fe, Co, Cu

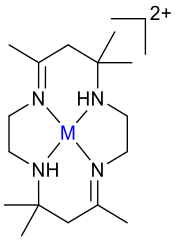

M = Co, Ni

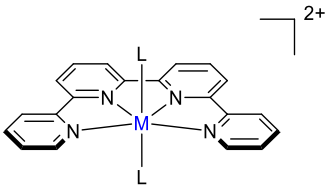

M = Fe, Co, Cu

(iii) Multinuclear metal complexes

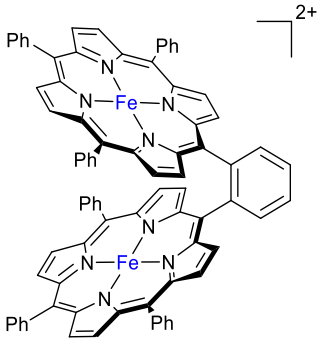

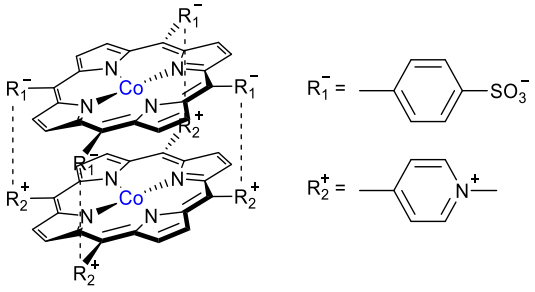

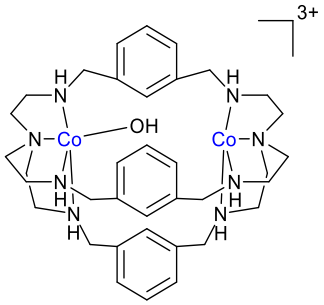

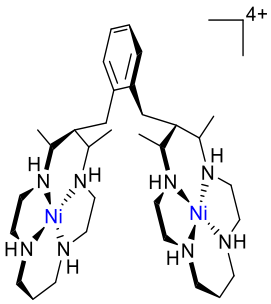

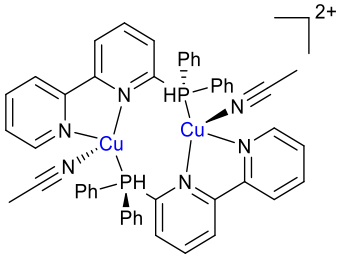

Metal-complex-based catalysts for formic acid dehydrogenation

The decomposition of HCOOH can proceed by two pathways: dehydrogenation to H_2 and CO_2, and dehydration to H_2O and CO ($HCOOH \rightarrow H_2O + CO$), which should be suppressed. Since the yield of each reaction pathway is affected by several parameters such as temperature, pressure, and solvent[47], the control over the reactions using suitable catalysts are required.

In 1967, the first report on homogeneous HCOOH dehydrogenation catalysts was published by Coffey, who tested several transition-metal complexes with phosphine ligands in refluxing acetic acid (118 °C) as the solvent.[48] Initial HCOOH dehydrogenation efficiency of up to TOF (turnover frequency) = 8900 h^{-1} was achieved with $[IrH_3(PPh_3)_3]$ catalyst. Subsequently, Rh-, Ir-, and Ru-based catalysts have been tested for the reaction.[49-55] In 2010, the first Fe-based catalyst with nitrogen and phosphine ligands was presented by Beller and co-workers.[56] From initial screening studies, $[Fe_3(CO)_{12}]$ in the presence of PPh_3 and 2,2':6',2"-terpyridine work as the most active catalyst for HCOOH dehydrogenation at temperatures above 100 °C. Interestingly, under visible light irradiation, the in situ generated catalyst was found to be active even at ambient temperature. Subsequently, several catalysts based on transition metals such as Mn, Fe, Co, Ni, Cu, Ru, and Ir have been tested for the reaction (some of them are summarized in Table 2).[57-70]

Important feature of HCOOH is that a carbon-neutral H_2 storage/release couple involving CO_2 and HCOOH (CO_2/HCOOH cycle) can be realized by recycling the formed CO_2 back into HCOOH. To date, several catalysts that allow for reversible CO_2 hydrogenation ($CO_2 + H_2 \rightarrow HCOOH$)/ HCOOH dehydrogenation have been reported.[58,59,63,64,67]

In recent years, it has also been reported that the synergistic effects between the distinct metal ions play an important role in the C-H elimination for the HCOOH dehydrogenation (Table 2(iii)).[71-73] However, examples of these multinuclear catalysts are limited, and further improvement in the activity is crucial for future practical applications.

Table 2. Molecular metal-based catalysts for HCOOH dehydrogenation.

(i) Noble metal complexes

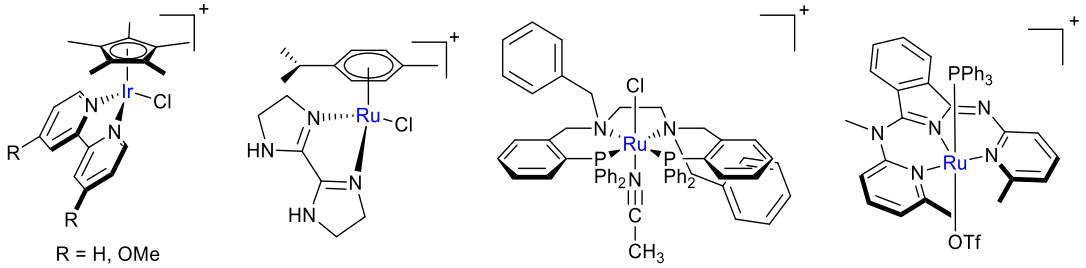

(ii) Non-noble metal complexes

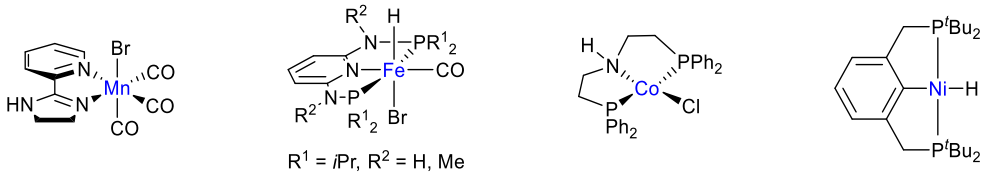

(iii) Multinuclear metal complexes

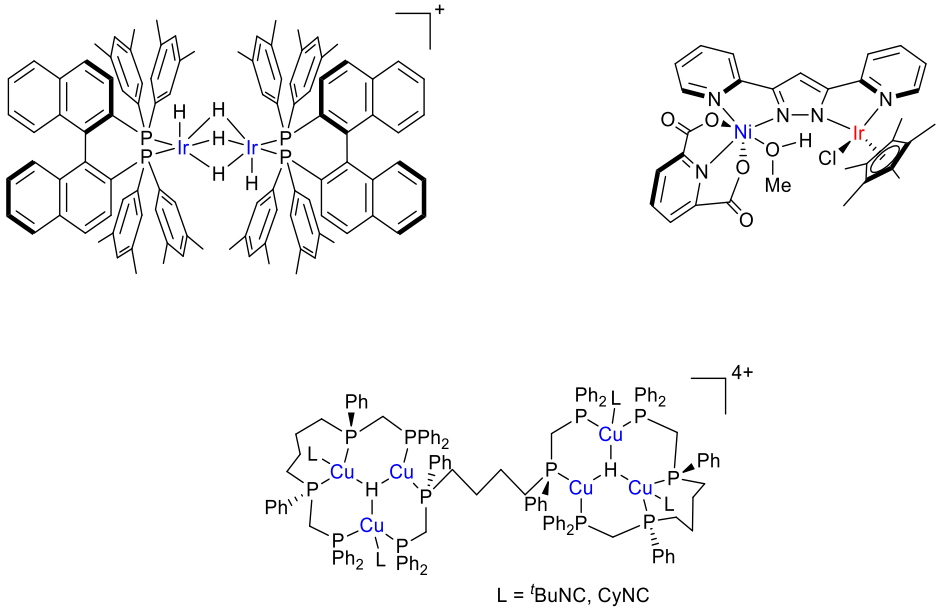

Multinuclear structures for small-molecular conversion

As mentioned earlier, the development of efficient catalysts for CO_2 reduction and HCOOH dehydrogenation is highly desired. These reactions are generally recognized as small-molecule conversion reactions. In nature, small-molecule conversion reactions efficiently proceed under ambient conditions using metalloenzymes as catalysts (Figure 2-4). Therefore, the extraction of important features of these metalloenzymes should be essential for obtaining keys to construct highly active artificial catalysts for small-molecule conversion reactions.

Oxygen evolving complex (OEC, Figure 2) in photosystem II catalyzes the light-driven water oxidation reaction ($2H_2O \rightarrow O_2 + 4H^+ + 4e^-$). The structure of OEC has been clarified by X-ray crystallographic and spectroscopic studies.[74,75] OEC has a multinuclear structure, a Mn_4CaO_4 cluster.

Nitrogenase catalyzes the nitrogen reduction ($N_2 + 6H^+ + 6e^- \rightarrow 2NH_3$) during the process of nitrogen fixation. Nitrogenase is a two-component system composed of the MoFe protein and the electron-transfer Fe protein[76-78]. MoFe protein contains two metal clusters: the MoFe cofactor ($MoFe_7S_9$ cluster, Figure 3), which provides the active site for substrate binding and reaction, and P-cluster (Fe_8S_7 cluster), involved in electron transfer. The alternative V- and Fe-type nitrogenases, where the Mo of MoFe cofactor is replaced by V and Fe, have also been discovered.[79]

Carbon monoxide dehydrogenase (CODH, Figure 4) catalyzes the reversible interconversion between CO_2 and CO ($CO_2 + 2H^+ + 2e^- \rightleftarrows CO + H_2O$) with high efficiency.[80,81] The active center of CODH is a multinuclear $NiFe_4S_4$ cluster (cluster C). In CODH, the CO_2 reduction reaction is initiated by a two-electron reduction of Ni^{II} to Ni^0 in cluster C. Then, CO_2 can be activated by the Ni center coordinating to the carbon atom of CO_2 as a Lewis base and one of the Fe centers binding to the oxygen atom of CO_2 as a Lewis acid. Such a dinuclear metal push-pull mechanism promotes C-O bond cleavage (Figure 5).

The specific feature of these enzymes is that their catalytically active centers are multinuclear metal complexes for promoting multi-electron transfer reactions. In addition, there exist sites for formation/cleavage of coordination bond(s). Due to these two key intrinsic features of the catalytic centers, the afore mentioned metalloenzymes can serve as highly active catalysts for small-molecule conversion reactions involving the transfer of multi-electron and the formation/cleavage of covalent bond(s). Therefore, artificial multinuclear metal complexes with these features are expected to be promising candidates for developing efficient artificial catalysts for small-molecule conversion reactions. However, a rational strategy to design and construct multinuclear metal complexes that

catalyze small-molecule conversion reactions has not been well established.

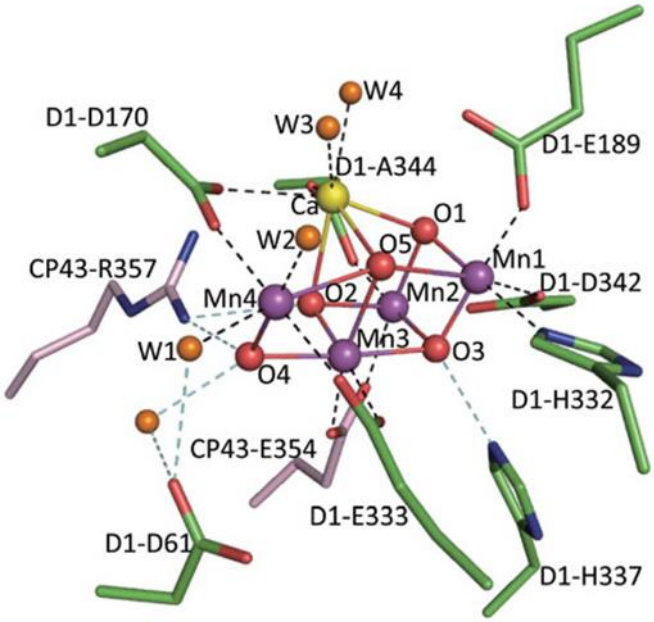

Figure 2. The structure of Mn_4CaO_5 cluster and its ligand environment in the OEC. Mn, purple; Ca, yellow; O, red; oxygen atoms in water molecules, orange; N, blue. Copyright 2011 Springer Nature.

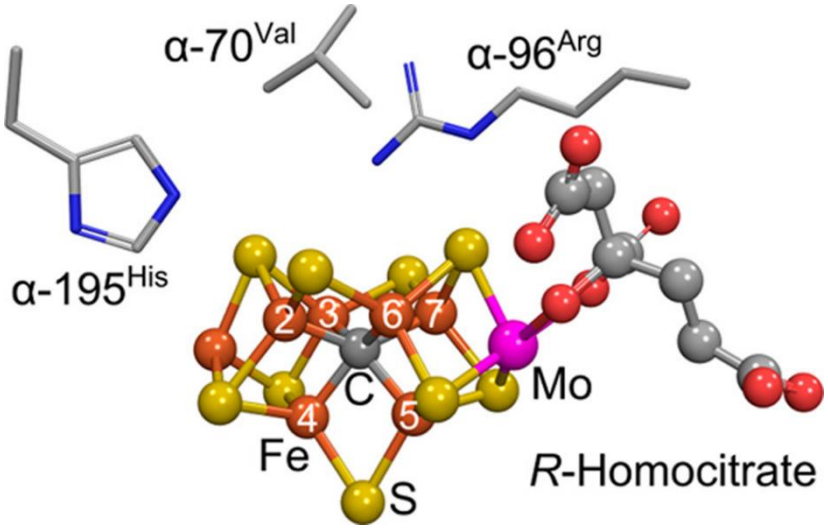

Figure 3. The structure of MoFe7S9 cluster and its ligand environment in the MoFe cofactor (nitrogenase). Mo, magenta; Fe, orange; S, yellow; C, gray; O, red; N, blue. Copyright 2014 American Chemical Society.

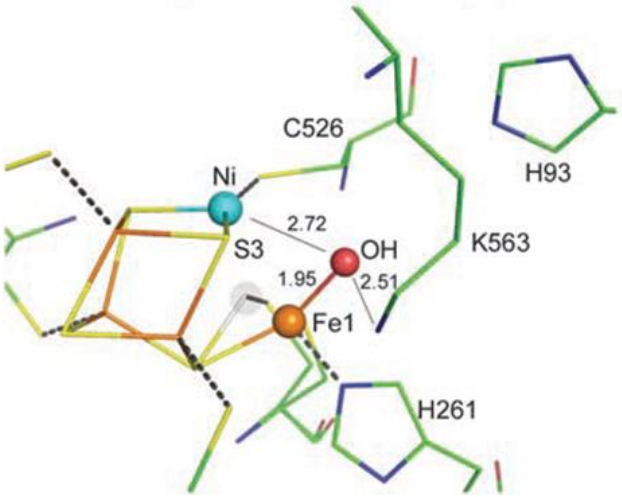

Figure 4. The structure of $NiFe_4S_4$ cluster and its ligand environment in the CODH. Ni, cyan; Fe, orange; S, yellow; O, red; N, blue. Copyright 2007 American Association for the Advancement of Science.

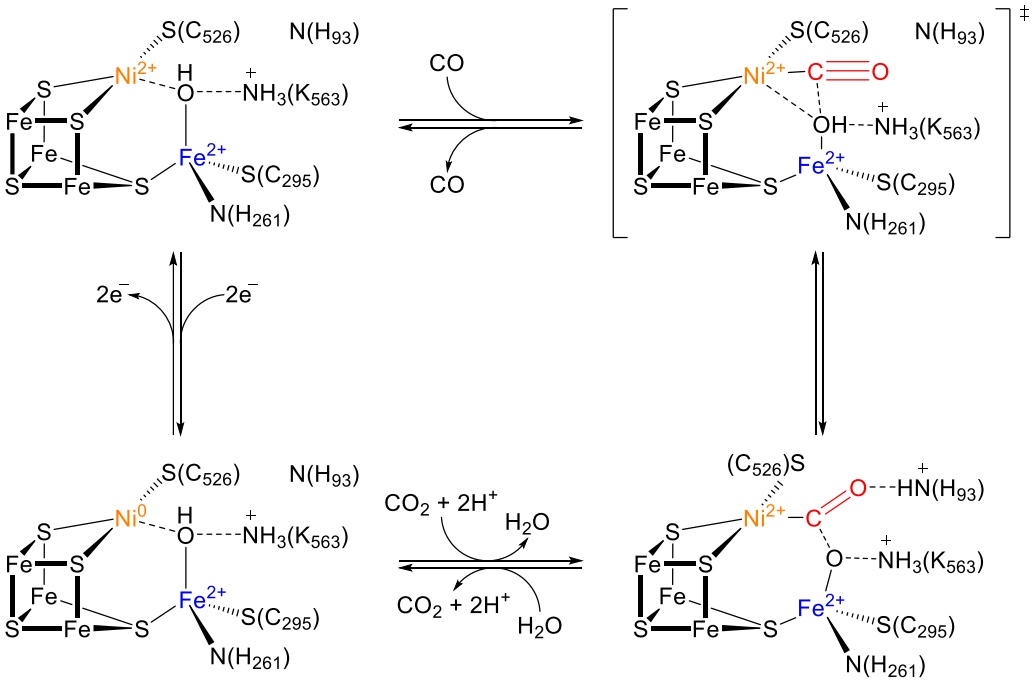

Figure 5. The mechanism of $NiFe_4S_4$ cluster in CODH for the reversible activation and conversion between CO_2 and CO.

Pentanuclear metal complexes

Our group has found that a pentanuclear iron complex composed of five iron ions and six bpp^- ligands ($[Fe_5O(bpp)_6]^{3+}$, **Fe5**, Hbpp = 3,5-bis(2-pyridyl)pyrazole) catalyzes the conversion of water molecules to dioxygen with an extremely high efficiency.[82] Notable feature of **Fe5** is that the complex has multinuclear structure suitable for multi-electron transfer and neighboring active sites suitable for a bond formation (Figure 6), which is conceptually identical to the catalytic center of metalloenzyme catalyzing small-molecule conversion reactions. It was also revealed by our group that these two features of **Fe5** were the origin of its high catalytic activity. These facts imply that the molecular scaffold composed of five metal ions and six Hbpp ligands can be an attractive platform to construct catalysts for small-molecule conversion. However, the catalytic activity of the scaffold is investigated only for a water oxidation reaction, and the applicability of the scaffold for other small-molecule conversion reactions has not been clarified.

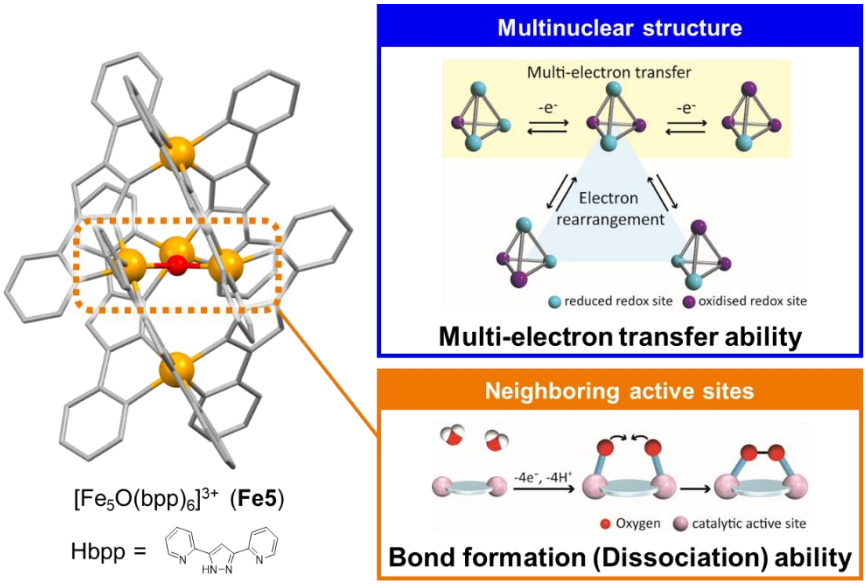

Figure 6. The structure of **Fe5** and the key for its reactivity.

Aim of this thesis

In this study, I aimed to construct the catalytic system for CO_2 utilization that produces CO and HCOOH by CO_2 reduction and H_2 by HCOOH dehydrogenation. I focused on the pentanuclear scaffold composed of five metal ions and six bpp^- organic ligands. Although the catalytic activity of the scaffold for an oxidation reaction, water oxidation, has been well-investigated, the catalytic activity for reduction reactions has not been explored. In addition, the effect of metal ion substitution in the pentanuclear scaffold on catalytic activity for small-molecule conversion reactions remained unclear. Based on the aforementioned considerations, I aimed to investigate the effect of metal ion substitution on the catalytic activity of the pentanuclear scaffold, and develop the new catalytic systems for CO_2 utilization.

Survey of this thesis

In chapter 1, I substituted metal ions of **Fe5** with cobalt ions and synthesized a novel pentanuclear cobalt complex (**Co5**). Electrochemical measurements indicate that **Co5** has multielectron transfer ability and works as a catalyst for CO_2 reduction. I also demonstrated that **Co5** reduces CO_2 to CO and HCOOH under electrochemical and photochemical conditions.

In chapter 2, I investigated the catalytic activity of **Co5** for photochemical HCOOH dehydrogenation reaction. As a result, the first catalytic cycle for hydrogen production based on the photochemical two-electron reduction of CO_2 and the dehydrogenation of HCOOH at ambient temperature was demonstrated using **Co5**. A series of mechanistic studies were performed to elucidate the mechanism responsible for the promotion of the photocatalytic cycle by **Co5**.

In chapter 3, I developed an efficient catalyst for a photocatalytic HCOOH/CO_2 cycle by metal ion substitution in a pentanuclear scaffold. I synthesized and characterized a pentanuclear copper complex (**Cu5**). **Cu5** served as a catalyst that drives both photochemical HCOOH production and dehydrogenation of HCOOH under ambient conditions with higher activity and selectivity than **Co5**.

References

1. Y. Yamazaki, H. Takeda and O. Ishitani, J. Photochem. Photobiol. C: Photochem. Rev., 2015, 25, 106.
2. H. Takeda, C. Cometto, O. Ishitani, M. Robert., ACS Catal., 2017, 7, 70.
3. Y. Kuramochi, O. Ishitani and H. Ishida, Coord. Chem. Rev., 2018, 373, 333.
4. K. Sordakis, C. Tang, L. K. Vogt, H. Junge, P. J. Dyson, M. Beller, G. Laurenczy, Chem. Rev., 2018, 118, 372.
5. H. Shulz, Appl. Catal. A-Gen., 1999, 186, 3.
6. D. Hildebrandt, D. Glasser, B. Hausberger, B. Patel, B. J. Glasser, Science, 2009, 323, 1680.
7. X. -F. Wu, H. Neumann, M. Beller, Chem. Soc. Rev., 2011, 40, 4986.
8. A. Schoenberg, I. Bartoletti, R. F. Heck, J. Org. Chem., 1974, 39, 3318.
9. J. Hawecker, J. -M. Lehn, R. Ziessel, J. Chem. Soc., Chem. Commun., 1983, 536.
10. Y. Kuramochi, J. Itabashi, K. Fukaya, A. Enomoto, M. Yoshida, H. Ishida, Chem. Sci., 2015, 6, 3063.
11. H. Ishida, K. Tanaka, T. Tanaka, Organometallics, 1987, 6, 181.
12. J. -M. Lehn, R. Ziessel, J. Organomet. Chem., 1990, 382, 157.
13. C. M. Bolinger, N. Story, B. P. Sullivan, T. J. Meyer, Inorg. Chem., 1988, 27, 4582.
14. H. Takeda, K. Koike, H. Inoue, O. Ishitani, J. Am. Chem. Soc., 2008, 130, 2023.
15. P. Kang, C. Cheng, Z. Chen, C. K. Schauer, T. J. Meyer, M. Brookhart, J. Am. Chem. Soc., 2012, 134, 5500.
16. C. M. Boudreaux, N. P. Liyanage, H. Shirley, S. Siek, D. L. Gerlach, F. Qu, J. H. Delcamp, E. T. Papish, Chem. Commun., 2017, 53, 11217.
17. S. K. Lee, M. Kondo, G. Nalamura, M. Okamura, S. Masaoka, Chem. Commun., 2018, 54, 6915.
18. S. K. Lee, M. Kondo, M. Okamura, T. Enomoto, G. Nakamura, S. Masaoka, J. Am. Chem. Soc., 2018, 140, 16899.
19. T. Watanabe, Y. Saga, K. Kosugi, H. Iwami, M. Kondo, S. Masaoka, Chem. Commun., 2022, 58, 5229.
20. M. Hammouche, D. Lexa, M. Momenteau, J. M. Savéant, J. Am. CHem. Soc., 1991, 113, 8455.
21. I. Bhugun, D. Lexa, J. -M. Savéant, J. Am. Chem. Soc., 1996, 118, 1769.
22. C. Costentin, S. Drouet, M. Robert, J. M. Savéant, Science, 2012, 338, 90.
23. C. Costentin, M. Robert, J. M. Savéant, A. Tatin, Proc. Natl. Acad. Sci. U. S. A., 2015, 112, 6882.

24. I. Azcarate, C. Constantin, M. Robert, J. M. Savéant, J. Am. Chem. Soc., 2016, 138, 16639.
25. J. Grodkowski, D. Behar, P. Neta, P. Hambright, J. Phys. Chem. A, 1997, 101, 248.
26. T. Dhanasekaran, J. Grodkowski, P. Neta, P. Hambright, E. Fujita, J. Phys. Chem. A, 1999, 103, 7742.
27. J. Bonin, M. Robert, M. Routier, J. Am. Chem. Soc., 2014, 136, 16768.
28. H. Rao, L. C. Schmidt, J. Bonin and M. Robert, Nature, 2017, 548, 74.
29. Z. Weng, J. Jiang, Y. Wu, Z. Wu, X. Guo, K. L. Materna, W. Liu, V. S. Batista, G. W. Brudbig, H. Wang, J. Am. Chem. Soc., 2016, 138, 8076.
30. K. Kosugi, H. Kashima, M. Kondo and S. Masaoka, Chem. Commun., 2022, 58, 2975.
31. B. J. Fisher, R. Eisenberg, J. Am. Chem. Soc., 1980, 102, 7361.
32. S. Matsuoka, K. Yamamoto, T. Ogata, M. Kusaba, N. Nakashima, E. Fujita, J. Am. Chem. Soc.,1993, 115, 601.
33. Z. Guo, S. Cheng, C. Cometto, E. Anxolabéhère-Mallart, S. -M. Ng, C. -C. Ko, G. Liu, L. Chen, M. Robert, T. -C. Lau, J. Am. Chem. Soc., 2016, 138, 9413.
34. Z. Guo, F. Yu, Y. Yang, C. F. Leung, S. -M. Ng, C. -C. Ko, C. Cometto, T. -C. Lau, M. Robert, ChemSusChem, 2017, 10, 4009.
35. V. S. Thoi, N. Kornienko, C. G. Margarit, P. Yang, C. J. Chang, J. Am. Chem. Soc., 2013, 135, 14413.
36. L. Chen, Z. Guo, X.-G. Wei, C. Gallenkamp, J. Bonin, E. Anxolabéhère-Mallart, K-C. Lau, T. -C. Lau, M. Robert, J. Am. Chem. Soc., 2015, 137, 10918.
37. D. Hong, Y. Tsukakoshi, H. Kotani, T. Ishizuka, T. Kojima, J. Am. Chem. Soc., 2017, 139, 6538.
38. H. Shirley, X. Su, H. Sanjanwala, K. Talukdar, J. W. Jurss, J. H. Delcamp, J. Am. Chem. Soc., 2019, 141, 6617.
39. E. A. Mohamed, Z. N. Zahran, Y. Naruta, Chem. Commun., 2015, 51, 16900.
40. Z. N. Zahran, E. A. Mohamed, Y. Naruta, Sci. Rep., 2016, 6, 24533.
41. O. Enoki, T. Imaoka, K. Yamamoto, Macromol. Symp., 2003, 204, 151.
42. T. Ouyang, H. -H. Huang, J. -W. Wang, D. -C. Zhong, T. -B. Lu, Angew. Chem. Int. Ed., 2017, 56, 738.
43. L. -M. Cao, H. -H. Huang, J. -W. Wang, D. -C. Zhong, T. -B. Lu, Green Chem., 2018, 20, 798.
44. T. Ouyang, H. -J. Wang, H. -H. Huang, J. -W. Wang, S. Guo, W. -J. Liu, D. -C. Zhong, T. -B. Lu, Angew. Chem. Int. Ed., 2018, 57, 16480.
45. R. J. Haines, R. E. Wittrig, C. P. Kubiak, Inorg. Chem., 1994, 33, 4723.

46. R. Angamuthu, P. Byers, M. Lutz, A. L. Spek, E. Bouwman, Science, 2010, 327, 313.
47. C. Wakai, K. Yoshida, Y. Tsujino, N. Matubayasi, M. Nakahara, Chem. Lett., 2004, 33, 572.
48. R. S. Coffey, Chem. Commun. (London), 1967, 923b.
49. J. C. Tsai, K. M. Nicholas, J. Am. Chem. Soc., 1992, 114, 5117.
50. D. Forster, G. R. Beck, J. Chem. Soc. D, 1971, 1072.
51. S. H. Strauss, K. H. Whitmire, D. F. Shriver, J. Organomet. Chem., 1979, 174, C59.
52. M. L. Man, Z. Zhou, S. M. Ng, C. P. Lau, Dalton Trans., 2003, 3727.
53. C. Fellay, P. J. Dyson, G. Laurenczy, Angew. Chem. Int. Ed., 2008, 47, 3966.
54. B. Loges, A. Boddien, H. Junge, J. R. Noyes, W. Baumann, M. Beller, Chem. Commun., 2009, 4185.
55. S. Fukuzumi, T. Kobayashi, T. Suenobu, J. Am. Chem. Soc., 2010, 132, 1496.
56. A. Boddien, B. Loges, F. Gärtner, C. Torborg, K. Fumino, H. Junge, R. Ludwig, M. Beller, J. Am. Chem. Soc., 2010, 132, 8924.
57. A. Boddien, F. Gärtner, R. Jackstell, H. Junge, A. Spannenberg, W. Baumann, R. Ludwig, M. Beller, Angew. Chem. Int. Ed., 2010, 49, 8993.
58. A. Boddien, F. Gärtner, C. Federsel, P. Sponholz, D. Mellmann, R. Jackstell, H. Junge, M. Beller, Angew. Chem. Int. Ed., 2011, 50, 6411.
59. S. -F. Hsu, S. Rommel, P. Eversfield, K. Muller, E. Klemm, W. R. Thiel, B. Plietker, Angew. Chem. Int. Ed., 2014, 53, 7074.
60. N. Scotti, R. Psaro, N. Ravasio, F. Zaccheria, RSC Adv., 2014, 4, 61514.
61. C. -H. Chang, M. -H. Chen, W. -S. Du, J. Gliniak, J. -H. Lin, H. -H. Wu, H. -F. Chan, J. -S. K. Yu, T. -K. Wu, Chem. Eur. J., 2015, 21, 6617.
62. S. M. Barrett, S. A. Slattery, A. J. M. Miller, ACS Catal., 2015, 5, 6320.
63. S. Enthaler, A. Brück, A. Kammer, H. Junge, E. Irran, S. Gülak, ChemCatChem, 2015, 7, 65.
64. F. Bertini, I. Mellone, A. Ienco, M. Peruzzini, L. Gonsalvi, ACS Catal., 2015, 5, 1254.
65. I. Mellone, N. Gorgas, F. Bertini, M. Peruzzini, K. Kirchner, L. Gonsalvi, Organometallics, 2016, 35, 3344.
66. C. Guan, D. -D. Zhang, Y. Pan, M. Iguchi, M. J. Ajitha, J. Hu, H. Li, C. Yao, M. -H. Huang, S. Min, J. Zheng, Y. Himeda, H. Kawanami, K. -W. Huang, Inorg. Chem., 2017, 56, 438.
67. J. B. Geri, J. L. Ciatti, N. K. Szymczak, Chem. Commun., 2018, 54, 7790.
68. W. Zhou, Z. Wei, A. Spannenberg, H. Jiao, K. Junge, H. Junge, M. Beller, Chem.

Eur. J., 2019, 25, 8459.
69. A. Léval, A. Agapova, C. Steinlechner, E. Alberico, H. Junge, M. Beller. Green Chem., 2020, 22, 913.
70. N. Lentz, A. Aloisi, P. Thuéry, E. Nicolas, T. Cantat, Organometallics, 2021, 40, 565.
71. T. Nakajima, Y. Kamiryo, M. Kishimoto, K. Imai, K. Nakamae, Y. Ura, T. Tanase, J. Am. Chem. Soc., 2019, 141, 8732.
72. D. Hong, Y. Shimoyama, Y. Ohgomori, R. Kanega, H. Kotani, T. Ishizuka, Y. Kon, Y. Himeda and T. Kojima, Inorg. Chem., 2020, 59, 11976.
73. Y. Sofue, K. Nomura and A. Inagaki, Chem. Commun., 2020, 56, 4519.
74. Y. Umena, K. Kawakami, J. -R. Shen, N. Kamiya, Nature, 2011, 473, 55.
75. M. Suga, F. Akita, M. Sugahara, M. Kubo, Y. Nakajima, T. Nakane, K. Yamashita, Y. Umena, M. Nakabayashi, T. Yamane, T. Nakano, M. Suzuki, T. Masuda, S. Inoue, T. Kimura, T. Nomura, S. Yonekura, L. -J. Yu, T. Sakamoto, T. Motomura, J. -H. Chen, Y. Kato, T. Noguchi, K. Tono, Y. Joti, T. Kameshima, T. Hatsui, E. Nango, R. Tanaka, H. Naitow, Y. Matsuura, A. Yamashita, M. Yamamoto, O. Nureki, M. Yabashi, T. Ishikawa, S. Iwata, J. -R. Shen, Nature, 2017, 543, 131.
76. M. M. Georgiadis, H. Komiya, P. Chakrabarti, D. Woo, J. J. Kornuc, D. C. Rees, Science, 1992, 257, 1653.
77. J. Kim, D. C. Rees, Science, 1992, 257, 1677.
78. B. M. Hoffman, D. Lukoyanov, Z. -Y. Yang, D. R. Dean, L. C. Seefeldt, Chem. Rev., 2014, 114, 4041.
79. R. R. Eady, Chem. Rev., 1996, 96, 3013.
80. T. I. Doukov, T. M. Iverson, J. Seravalli, S. W. Ragsdale, C. L. Drennan, Science, 2002, 298, 567.
81. J. -H. Jeoung, H. Dobbek, Science, 2007, 318, 1461.
82. M. Okamura, M. Kondo, R. Kuga, Y. Kurashige, T. Yanai, S. Hayami, V. K. K. Praneeth, M. Yoshida, K. Yoneda, S. Kawata, S. Masaoka, Nature, 2016, 530, 465.

Chapter 1

Effect of metal ion substitution on the catalytic activity of a pentanuclear metal complex

Introduction

Multinuclear metal complexes are attractive materials due to not only their fascinating structure[1-3] but also their unique redox,[4-6] magnetic[7,8] and photochemical[9,10] properties and reactivity,[11-14] which differ from those of mononuclear complexes. Multinuclear structures in metalloenzymes work as important catalysts for small-molecule conversion reactions involving multielectron transfer.[15-21] Therefore, metal complexes with multinuclear structures are expected to be promising candidates for developing efficient artificial catalysts for such reactions. However, a rational strategy to design and construct multinuclear metal complexes that catalyze small-molecule conversion reactions has not been well established.

Given that small-molecule conversion requires transfer of multiple electrons and cleavage/formation of covalent bond(s), catalysts to facilitate these two processes must be developed. Recently, our group found that a pentanuclear iron complex composed of five iron ions and six bpp^- ligands ($[Fe_5O(bpp)_6]^{3+}$, **Fe5**, Hbpp = 3,5-bis(2-pyridyl)pyrazole) catalyzes the conversion of water molecules to dioxygen ($2H_2O \rightarrow O_2 + 4H^+ + 4e^-$) with high efficiency.[22] It was also demonstrated that multinuclear structure and coordinatively unsaturated sites are the keys to achieving rapid multielectron transfer and smooth O-O bond formation, respectively. These results imply that the molecular scaffold constructed by five metal ions and six bpp^- ligands is an attractive platform to construct catalysts for small-molecule conversion.

In this chapter, I show the synthesis, characterization, and catalytic activity of a pentanuclear cobalt complex composed of five cobalt ions and six bpp^- ligands (**Co5**). Although **Fe5** exhibited multi-electron oxidation ability, the introduction of cobalt ions into the same molecular scaffold endowed the complex with multi-electron reduction ability. Electrochemical measurements of **Co5** under a CO_2 atmosphere indicated the catalytic activity of the complex for CO_2 reduction. Furthermore, photoirradiation of a solution containing **Co5** and a photosensitizer under CO_2 resulted in the formation of CO, and the role of **Co5** as a CO_2 reduction catalyst was confirmed. Although there exist many examples of mononuclear[23-44] or dinuclear[45-47] metal complexes for CO_2 reduction, there are a few reports on multinuclear-metal-complex based systems[48,49]. The present study offers a rare example of multinuclear-metal-complex catalyst for CO_2 reduction.

Results and discussions

Synthesis and characterizations

A pentanuclear cobalt complex (**Co5**) was synthesized according to the procedure shown in Scheme 1. Aqueous solution of NaOH (1 M, 0.48 mL) was added to the methanol solution (4 mL) of Hbpp (0.48 mmol, 107 mg). $Co(CH_3COO)_2 \cdot 4H_2O$ (40 mmol, 100 mg) was then added to the reaction mixture and stirred at 40 °C for 10 minutes. A few drops of saturated aqueous $NaBF_4$ solution was added to the reaction mixture, and a small portion of water was added to the solution. The solution was kept in a refrigerator for 1 h to generate a brown precipitate. The precipitate was collected by filtration, washed with water and dried under vacuum. The obtained precipitate was dissolved in acetonitrile and subjected to vapor diffusion in diethyl ether to afford brown crystals of $[Co^{II}_5OH(bpp)_6](BF_4)_3 \cdot 2H_2O$. The crystals were collected by filtration and dried under vacuum to afford the targeted complex in 52% yield. The complex was characterized by electrospray ionization time-of-flight mass spectroscopy (ESI-TOF-MS), elemental analysis, and single crystal X-ray structural analysis. ESI-TOF-MS: m/z: 546 $[Co_5OH(bpp)_6]^{3+}$. Elemental analysis calcd. (%) for $C_{78}H_{59}Co_5F_{12}N_{24}O_3B_3$: C,48.40; H, 3.07; N, 17.37. Found: C, 48.35; H, 3.13; N, 17.32.

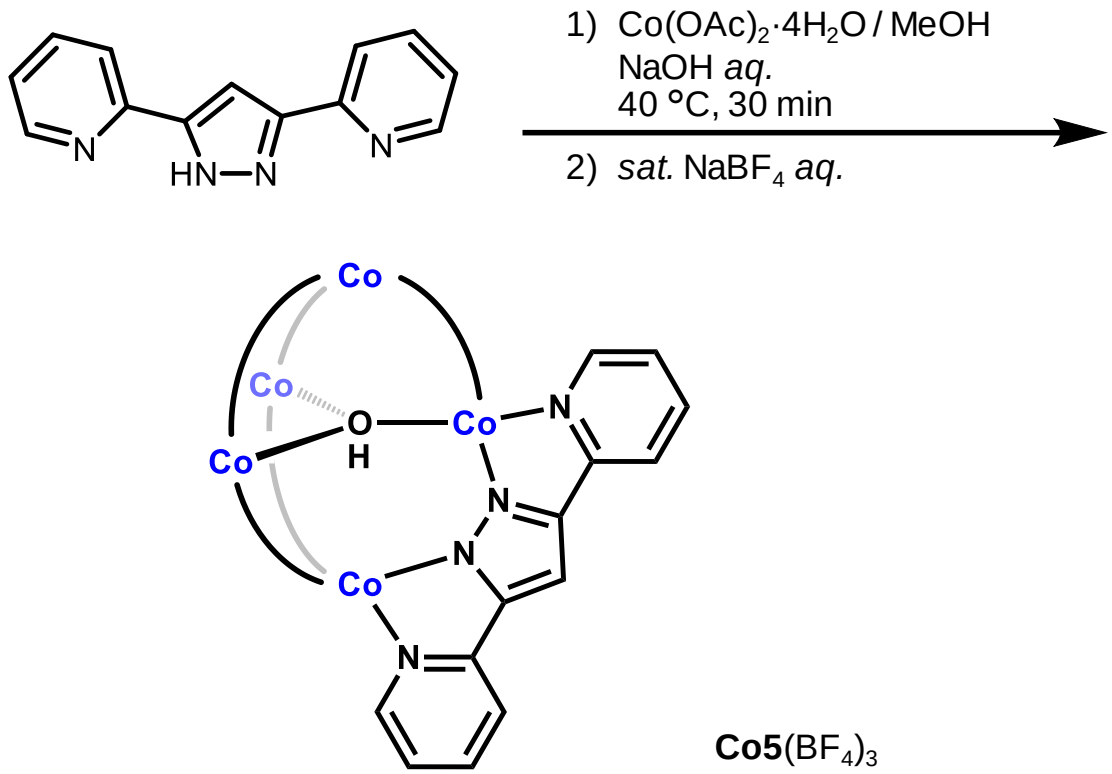

Scheme 1. Synthetic scheme of **Co5**$(BF_4)_3$.

Figure 1 shows an ORTEP diagram of **Co5** determined by single-crystal X-ray structural analysis. **Co5** crystallizes in the $P\,2_1/n$ space group, and the asymmetric unit of the structure contains one **Co5,** three BF_4 anions, one water, one MeCN and two diethyl ether molecules. Therefore, the total charge of **Co5** was determined to be +3. **Co5** exhibits quasi-D_3 symmetry and consists of a triangle core wrapped by two [Co(μ-bpp)$_3$] units. The two metal ions at the apical positions (M_{api}) are hexa-coordinated structures with distorted octahedral geometries, whereas the three metal ions in the triangular core (M_{core}) exhibit penta-coordinated structures with distorted trigonal bipyramidal geometries. The average bond distance between M_{api} and the nitrogen atoms of the [M(μ-bpp)$_3$] units of **Co5** is 2.149(5) Å (Table 2), which is the typical value for hexacoordinated Co(II) ions.[50] The average bond distance between M_{core} and the oxygen atom of the bridging moiety is 2.009(4) Å, which is larger than that of **Fe5**$(BF_4)_3$ (1.961(3) Å). In IR spectrum of **Co5**, the peak at 3500 cm^{-1} assigned with O-H stretching mode was observed, whereas this peak was not observed in **Fe5**. (Figure 2) These observations indicate that the bridging ligand at the triangle core of **Co5** is OH^-, which is different from the core structure of **Fe5**, which has an oxo (O^{2-}) bridging moiety. Based on these results, the structure of **Co5** has been determined to be **$[Co^{II}_5OH(bpp)_6]^{3+}$**.

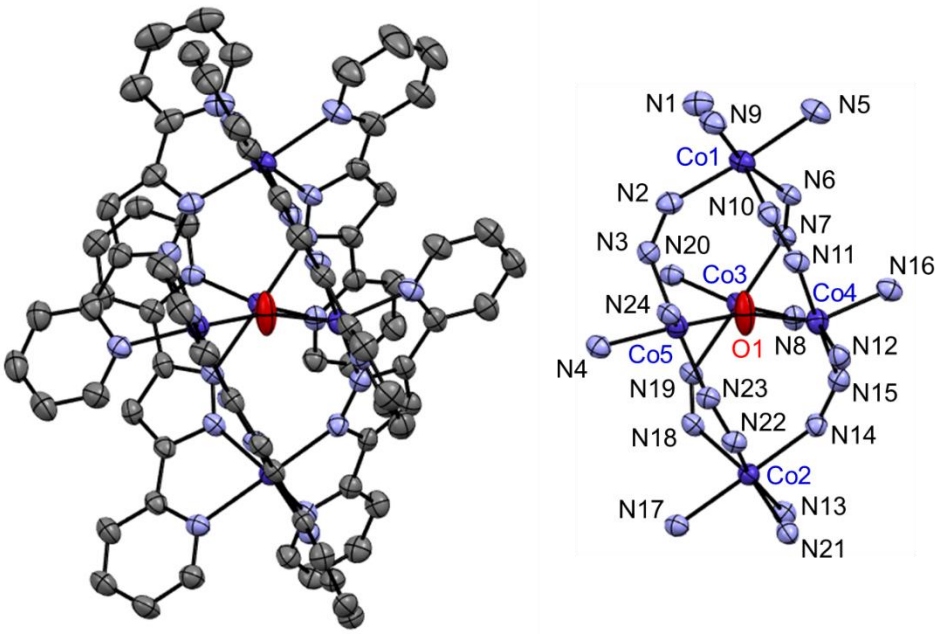

Figure 1. ORTEP drawings of the cationic moiety (left) and core structure (right) of **Co5**$(BF_4)_3$. The atoms are represented by the following colors: Co, blue; O, red; N, purple; C, grey. Hydrogen atoms and crystal solvent molecules are omitted for clarity.

Table 1. Summary of crystallographic data for **Co5**$(BF_4)_3$.

	$[Co_5OH(bpp)_6](BF_4)_3$
formula	$C_{78}H_{55}B_3Co_5F_{12}N_{24}O$
crystal system	monoclinic
space group	$P\,2_1/n$
a /Å	15.2146(6)
b /Å	22.3484(8)
c /Å	26.8017(12)
β /°	102.122(4)
V /Å^3	8910.0(6)
Z	4
R_1	0.0720
wR_2	0.2172
GooF	1.027

Table 2. Selected bond lengths of **Co5**$(BF_4)_3$.

	bond	**length /Å**
$d(M_{api}\text{-}N)$	Co1-N1	2.198(5)
	Co1-N2	2.108(5)
	Co1-N5	2.186(5)
	Co1-N6	2.103(4)
	Co1-N9	2.182(5)
	Co1-N10	2.104(4)
	Co2-N13	2.195(5)
	Co2-N14	2.100(5)
	Co2-N17	2.175(5)
	Co2-N18	2.118(5)
	Co2-N21	2.195(5)
	Co2-N22	2.120(5)
average		**2.149(5)**
$d(M_{core}\text{-}N)$	Co3-N3	2.054(5)
	Co3-N4	2.072(5)
	Co3-N15	2.055(5)
	Co3-N16	2.086(4)
	Co4-N7	2.049(4)
	Co4-N8	2.073(5)
	Co4-N19	2.073(5)
	Co4-N20	2.070(5)
	Co5-N11	2.055(4)
	Co5-N12	2.084(4)
	Co5-N23	2.056(4)
	Co5-N24	2.072(5)
average		**2.067(5)**
$d(M_{core}\text{-}O)$	Co3-O1	1.997(4)
	Co4-O1	2.017(4)
	Co5-O1	2.014(4)
average		**2.009(4)**

Table 3. Selected angles of **Co5**$(BF_4)_3$.

	bond	**angle /deg**
core angle	Co3-O1-Co4	120.4(2)
	Co3-O1-Co5	120.3(2)
	Co4-O1-Co5	118.7(2)
average		**119.8(2)**

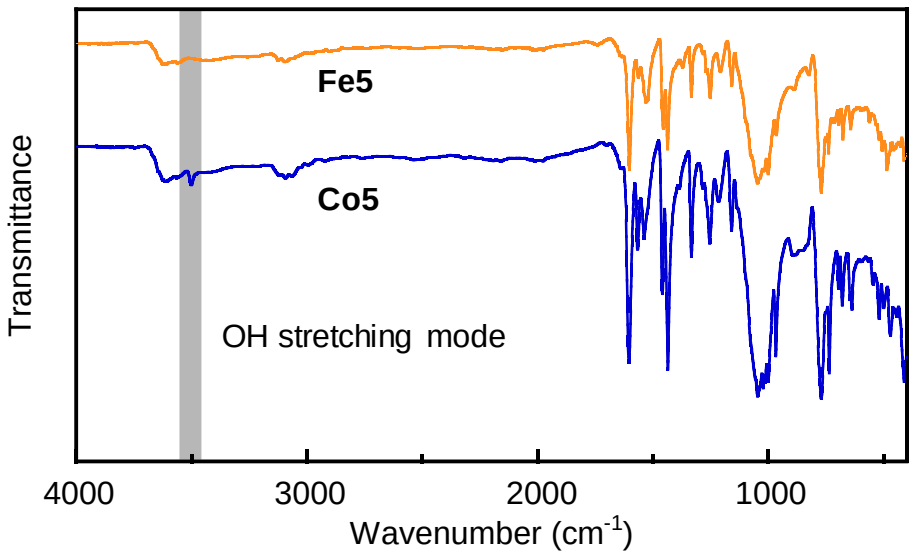

Figure 2. IR spectra of **Fe5**$(BF_4)_3$ (orange line) and **Co5**$(BF_4)_3$ (blue line).

Electrochemical measurements

To explore the electron-transfer ability of **Co5**, cyclic voltammetry was performed. In a cyclic voltammogram (CV) of **Co5** under an Ar atmosphere (Figure 3, blue line), the complex displayed two reversible oxidation waves at −0.30 and −0.11 V (*vs.* ferrocene/ferrocenium (Fc/Fc^+)) and three reversible reduction waves at −1.72, −1.96, and −2.19 V. This redox behavior of **Co5** is completely distinct from that of **Fe5**, which shows four reversible oxidation waves and one reversible reduction wave (Figure 3, orange line), indicating that **Co5** has redox properties suitable for reductive reactions.

It should be noted that the relevant complex composed of redox inactive metal ions, $[Zn^{II}_5OH(bpp)_6]^{3+}$ (**Zn5**), did not show any redox peaks in the potential region of 1.2 - −2.3 V (see Experimental section), indicating that ligand-based redox process does not occur both in **Co5** and **Zn5**. The redox peaks of **Co5** were assigned by comparing the CV of **Co5** with those of heterometallic pentanuclear metal complexes,[51] that composed of bpp^-, ruthenium ions at apical positions, and first-raw transition metal ions at the triangular core. The heterometallic complex bearing ruthenium and zinc ions (**Ru2Zn3**, see Experimental section) exhibited two reversible redox waves at $E_{1/2}$ = 0.35 and 0.51 V (vs. Fc/Fc^+), and these waves were attributed to the sequential oxidation of the ruthenium ions at the apical positions because zinc ions are redox inactive. In the CVs of heterometallic complex bearing ruthenium and cobalt ions (**Ru2Co3**) and **Co5** (see Experimental section), two reversible oxidation and three reversible reduction waves were observed. The $E_{1/2}$ values of the oxidation waves of **Ru2Co3** (0.36 and 0.52 V) are almost identical to those of **Ru2Zn3**, indicating that these can be attributed to the oxidation of the ruthenium ions. The redox potentials of the reduction waves of **Ru2Co3** and **Co5** were also quite similar ($E_{1/2}$ = −1.71, −1.98, and −2.24 V for **Ru2Co3** and −1.72, −1.96, and −2.19 V for **Co5**), and thus, these waves are assignable to the reduction of the cobalt ions in the triangular core. Therefore, the oxidation waves are attributed to the oxidation of cobalt ions (Co^{III}/Co^{II}) at the apical positions, and the reduction waves are assigned to the reduction of the cobalt ions (Co^{II}/Co^{I}) at the triangle core.

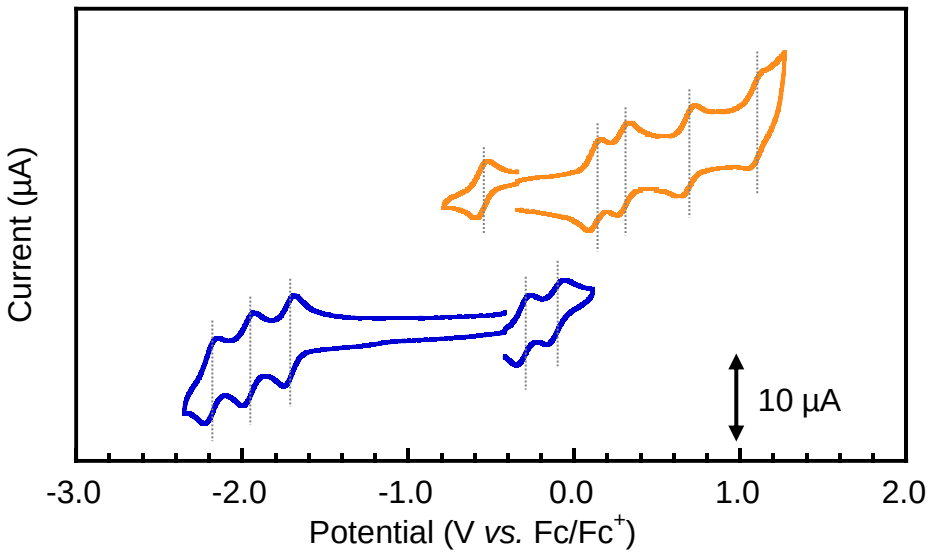

Figure 3. Cyclic voltammograms of 0.2 mM solutions of **Co5** (blue line) and **Fe5** (orange line) under Ar in MeCN containing 0.1 M TBAP. The CVs were measured using a GC electrode at a scan rate of 100 mVs^{-1}.

Encouraged by the aforementioned results, the electrocatalytic activity of **Co5** for CO_2 reduction was examined. As shown in Figure 4, the CV of **Co5** measured under CO_2 using anhydrous acetonitrile as a solvent exhibited a large irreversible current at approximately E_{pc} = −2.2 V. Notably, the intensity of the irreversible current further increased in the presence of trifluoroethanol (TFE) as a proton source. These results indicate the electrocatalytic activity of the complex for CO_2 reduction.

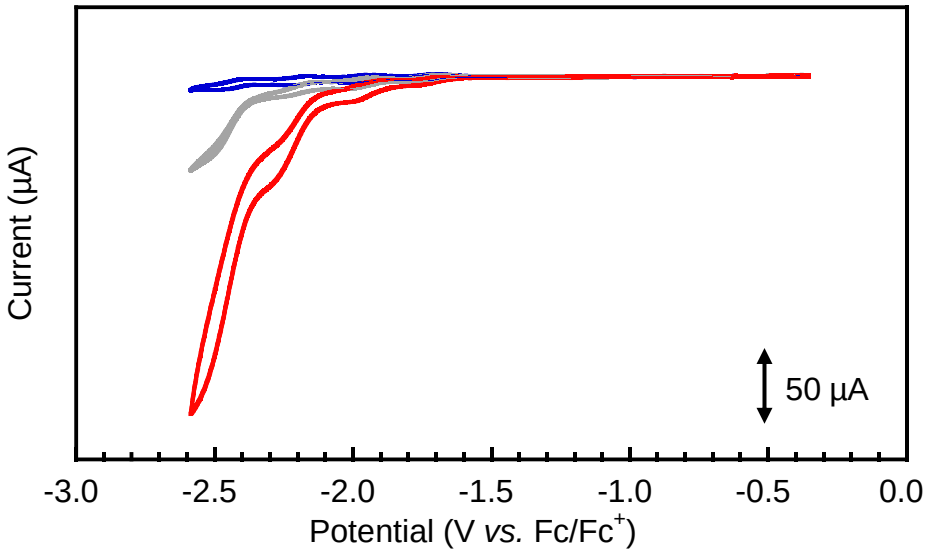

Figure 4. Cyclic voltammograms of 0.2 mM solutions of **Co5** under Ar (blue line), CO_2 (grey line) and CO_2 in the presence of 10 % trifluoroethanol (red line) in MeCN containing 0.1 M TBAP. The CVs were measured using a GC electrode at a scan rate of 50 mVs^{-1}.

Electrocatalytic reaction

To verify the electrocatalytic activity of **Co5** for CO_2 reduction, the controlled-potential electrolysis (CPE) was performed. In the CPE conducted at −2.5 V (vs. Fc/Fc^+), approximately 0.98 C of charge passed during 1 h of electrolysis (Figure 5, red line, Table 4, No. 1), and the formation of CO (0.09 μmol) and HCOOH (0.22 μmol) was confirmed. Added 5 % TFE as a proton source in the system, the amount of evolved CO (0.11 μmol) increased (Figure 5, blue line, Table 4, No. 2). In the absence of **Co5**, no CO_2 reduction product was observed (Figure 5, black line, Table 4, No. 3). These results clearly indicate that **Co5** can promote electrochemical CO_2 reduction.

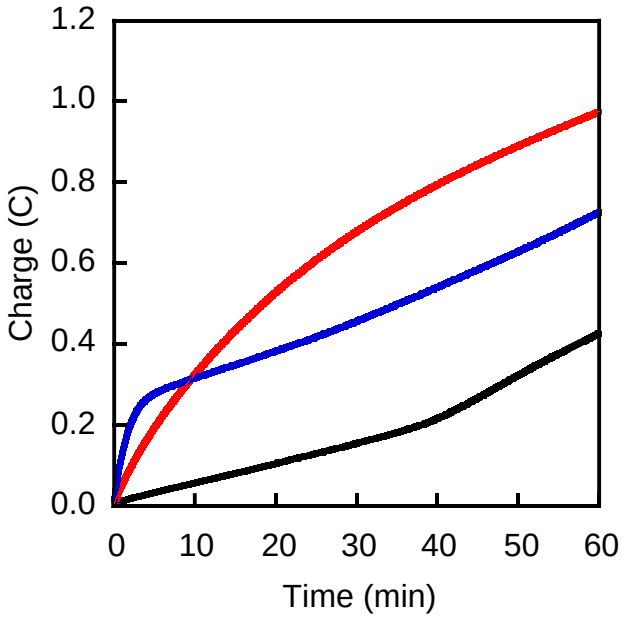

Figure 5. The result of CPE of 0.2 mM **Co5** (red line), **Co5** in the presence of 5 % trifluoroethanol (blue line) or in the absence of **Co5** (black line) in 0.1 M TBAP/MeCN under CO_2 at −2.5 V (vs. Fc/Fc^+) for 1 h. The CPE experiments were carried out using a GC plate as a working electrode.

Table 4. Summary of CPE experiments.[a]

No.	Catalyst	TFE (%)	Charge (C)	Product (μmol)		
				CO	H_2	HCOOH
1	**Co5**	-	0.98	0.09	0.05	0.22
2	**Co5**	5	0.73	0.11	0.19	0.08
3	-	-	0.43	0	0.01	0

[a] Conditions: 0.2 mM **Co5**, applied voltage: −2.5 V (vs. Fc/Fc^+), duration: 1 h.

Photochemical CO_2 reduction

The catalytic activity of **Co5** for photocatalytic CO_2 reduction was investigated. A photocatalytic CO_2 reduction experiment was conducted in 2 mL of a CO_2-saturated *N,N*-dimethylacetamide (DMA)/trifluoroethanol (TFE) (17:3, v/v) solution containing **Co5** (30 μM) as a catalyst, 1,3-dimethyl-2-phenyl-2,3-dihydro-1*H*-benzo[d]imidazole (BIH, 0.1 M) as a sacrificial electron donor (SD) and $Ir(ppy)_3$ (Hppy = 2-phenylpyridine, 150 μM) as a photosensitizer (PS) under visible-light irradiation (blue LED, wavelength λ = 420 nm). As shown in Figure 6, the evolution of CO (0.27 μmol), HCOOH (0.14 μmol) and H_2 (0.22 μmol) was observed after 3 h of photoirradiation. Hydrogen production ability was investigated in Chapter 2.

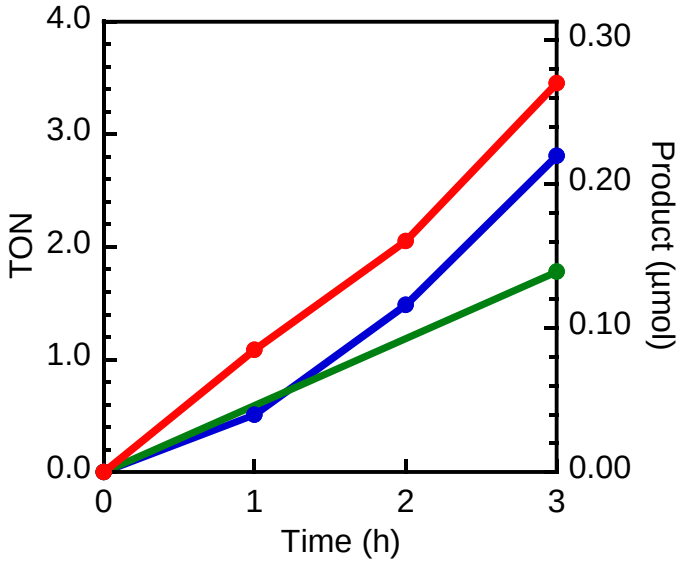

Figure 6. Photocatalytic production of CO (red line), HCOOH (green line) and H_2 (blue line) in a CO_2-saturated DMA/TFE (17:3, v/v) solution containing 30 μM **Co5**, 150 μM $Ir(ppy)_3$ and 0.1 M BIH.

To verify the role of each component in the photoreaction, a series of control experiments were carried out. No CO_2 reduction product was observed when the reaction was performed under argon, in the dark, without **Co5**, without $Ir(ppy)_3$, or without BIH (Table 5), showing that all components are required for the catalysis. The necessity of visible-light and $Ir(ppy)_3$ indicates that $Ir(ppy)_3$ functions as the photosensitizer because the complex has a strong absorption band in the visible region, and is frequently used as a photosensitizer in many photocatalytic systems.[28,30-32,40] **Co5** should serve as a catalyst to reduce CO_2 as also evidenced by electrochemical measurements (*vide supra*). The role of BIH should be a sacrificial electron donor as evidenced in previous reports.[33,39,40] These show that CO_2 is the substrate, **Co5** is the catalyst, $Ir(ppy)_3$ is the photosensitizer, and BIH serves as a sacrificial electron donor in our system.

Table 5. Control experiments for photocatalytic CO_2 reduction by **Co5** for 2h.[a,b]

No.	[**Co5**] (μM)	[PS] (μM)	[SD] (M)	light (nm)	gas	CO (μmol)
1	30	150	0.1	420	CO_2	0.10
2	-	150	0.1	420	CO_2	0
3	30	-	0.1	420	CO_2	0
4	30	150	-	420	CO_2	0
5	30	150	0.1	dark	CO_2	0
6	30	150	0.1	420	Ar	0

[a] PS = photosensitizer: $Ir(ppy)_3$, SD = sacrificial electron donor: BIH.

[b] All experiments were carried out in DMA/TFE (17:3, v/v) at 20 °C.

Isotopic labeling experiments were performed and peaks were observed at *m/z* = 28 (^{12}CO) and 29 (^{13}CO) under $^{12}CO_2$ and $^{13}CO_2$ atmosphere respectively (Figure 7). It was also confirmed that the CO originated from CO_2 reduction.

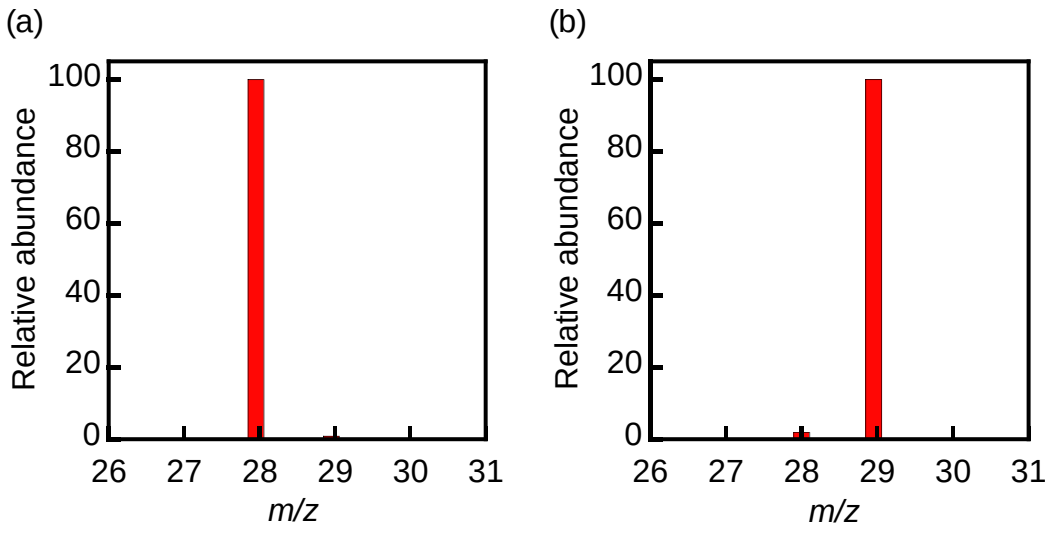

Figure 7. Mass spectra of CO generated under (a) $^{12}CO_2$ or (b) $^{13}CO_2$ using a DMA/TFE (17:3, v/v) solution containing 30 μM **Co5**, 150 μM $Ir(ppy)_3$ and 0.1 M BIH at 20 °C upon irradiation with a blue LED (420 nm) for 2h.

Mechanistic studies

To elucidate the electron-transfer process to **Co5**, the role of the photosensitizer was investigated.

In general, a PS can possibly transfer electrons from an electron donor to a catalyst in two different ways: oxidative quenching or reductive quenching for producing the reduced species (Figure 8). In oxidative quenching, the exited PS (PS*) is quenched by Cat and PS is regenerated by a sacrificial electron donor (SD). In reductive quenching, on the other hand, the PS* is quenched by SD to be one-electron-reduced species, which reduces Cat. The quenching rate constant (k_q) is used as an indication of the photochemical electron transfer reactions. The value of k_q can be estimated from Stern-Volmer plots (Eq. 1), which is the plots of relative emission intensity versus the concentration of the quencher (Cat or SD):

$$\frac{I_0}{I} = 1 + k_q \tau_0 [Q] \qquad (1)$$

where I_0 and I represent the emission intensities in the absence and presence of the quencher, τ_0 represents the lifetime of the excited state of the photosensitizer.

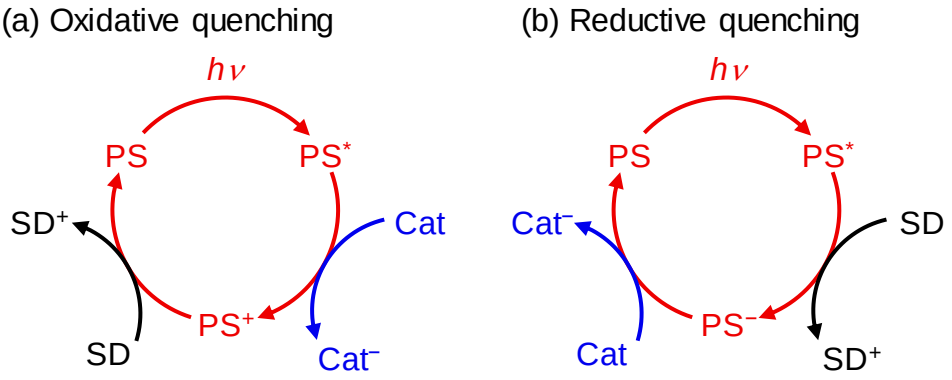

Figure 8. Two photoinduced electron transfer pathways: (a) oxidative quenching and (b) reductive quenching.

There are two possible pathways for electron transfer to **Co5**. The first pathway is the reductive quenching of $Ir(ppy)_3$ by BIH and the subsequent reduction of **Co5** by formed one-electron reduced species of $Ir(ppy)_3$. The second pathway is the oxidative quenching of $Ir(ppy)_3$ by **Co5**, resulting in the one-electron reduced state of **Co5**. To elucidate the photoinduced electron transfer pathway during catalysis, I examined the rates of quenching of the excited-state photosensitizer $Ir(ppy)_3$ by **Co5** (oxidative quenching) and BIH (reductive quenching) using Stern–Volmer plots. Upon increasing the concentration of **Co5**/BIH in a solution of $Ir(ppy)_3$, emission quenching was observed (Figure 9). The corresponding quenching rate constants for the oxidative and reductive quenching pathways were determined to be k_q = 6.6 x 10^9 and 5.5 x 10^6 M^{-1} s^{-1}, respectively. Considering that the concentration of BIH is approximately 10^3 times higher than that of **Co5** in the proposed photocatalytic reaction, the rates of the two quenching pathways are comparable.

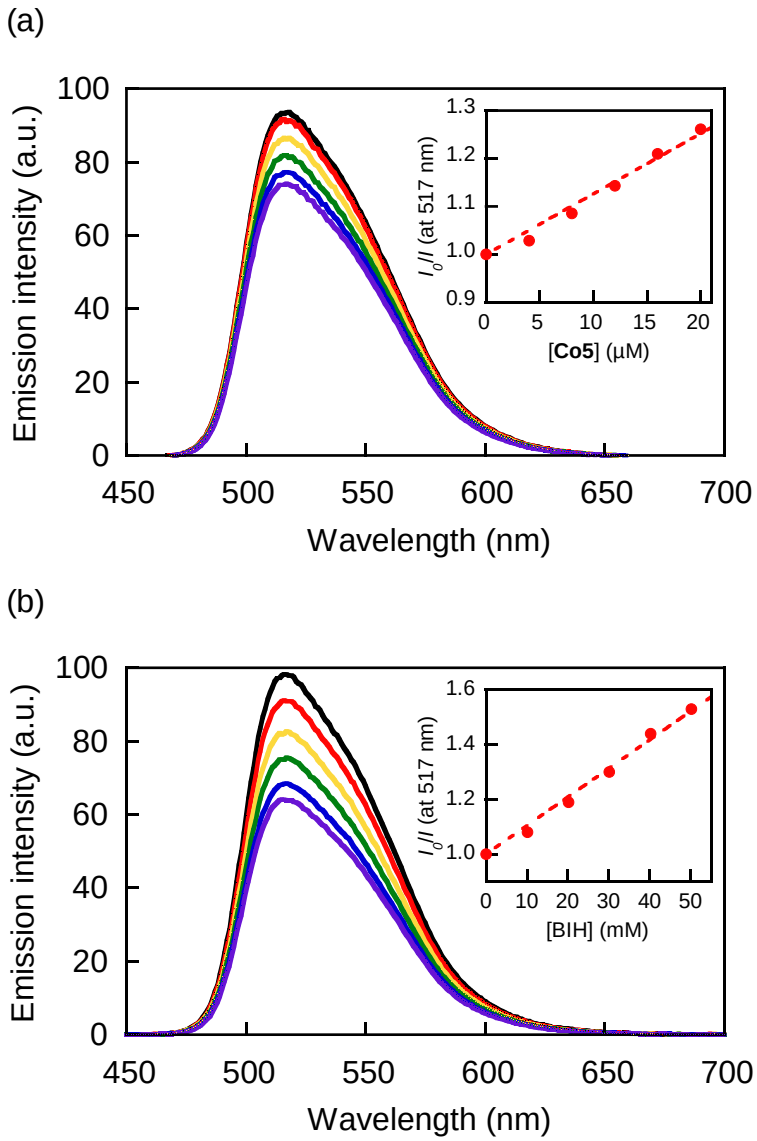

Figure 9. $Ir(ppy)_3$ emission quenching after excitation at 420 nm. (a) Upon increasing concentration of **Co5** in a 150 μM *N,N*-dimethylacetamide solution of $Ir(ppy)_3$. (b) Upon increasing concentration of BIH in a 150 μM *N,N*-dimethylacetamide solution of $Ir(ppy)_3$. (insets) Results of Stern-Volmer analyses, where I_0/I is the emission intensity without quencher (I_0) divided by the emission intensity with a known concentration of quencher (I). Luminescence spectra was recorded on Shimadzu RF5300PC spectrofluorophotometer.

Based on the results described above as well as those of previous reports on the CO_2 reduction, a possible mechanism for the described catalytic system based on **Co5** is proposed (Scheme 2). First, in the oxidative quenching pathway, **Co5** is reduced by exited $Ir(ppy)_3$ (Ir^{III*}). On the other hand, reduced $Ir(ppy)_3$ (Ir^{II}) is formed by the one-electron donation of BIH, and Ir^{II} reduces **Co5**. The one-electron reduced **Co5** (**Co5**$^-$) further receives an electron from the photosensitizer and reduces CO_2 to HCOOH or CO.

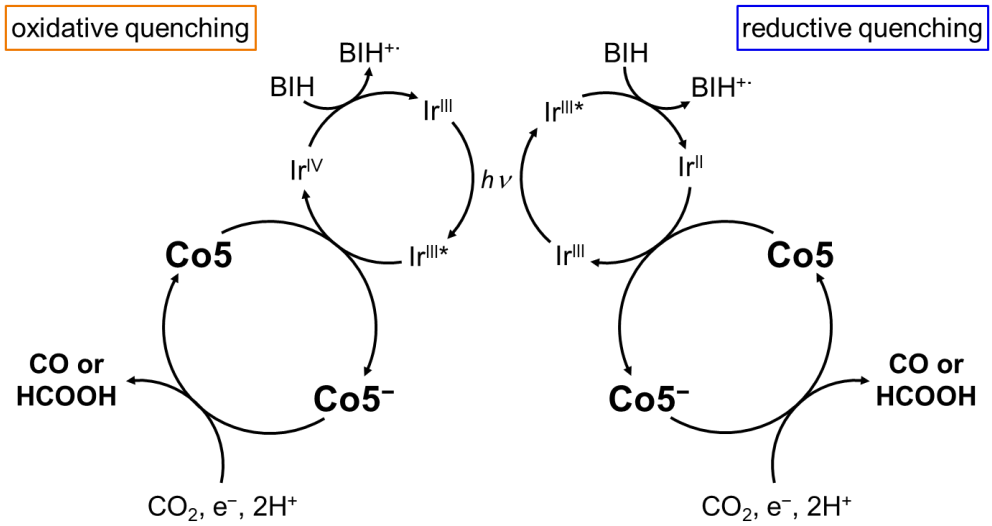

Scheme 2. Proposed mechanism of the CO_2 reduction mediated by **Co5**. (left) Oxidative quenching pathway and (right) reductive quenching pathway.

Optimization

Reaction conditions were also optimized, and the maximum turnover numbers of CO and HCOOH production reached 58.4 and 55.7 (Figure 10, red line and green line), respectively, when the **Co5** concentration was decreased to 1 μM and light source was changed into a xenon lamp equipped with 420 nm long pass filter and CM-1 cold mirror (wavelength $420 \leq \lambda \leq 750$ nm). In this optimized condition, the formation of H_2 (TON = 61.8, Figure 10, blue line) was also detected.

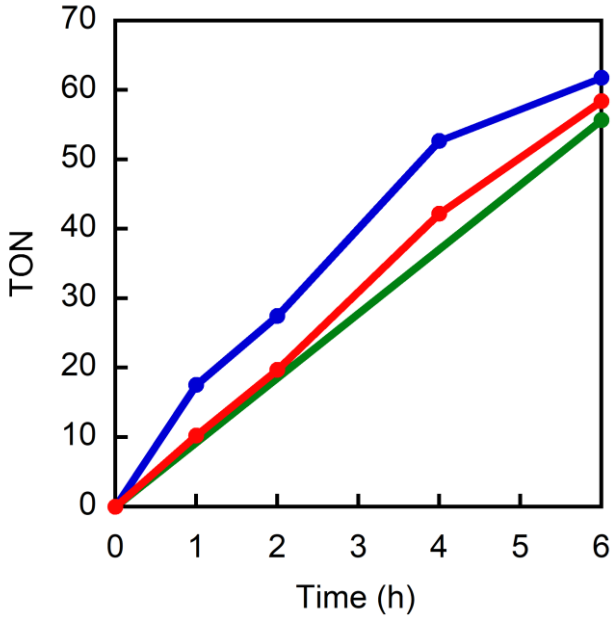

Figure 10. Photocatalytic production of CO (red line), HCOOH (green line), and H_2 (blue line) in a CO_2 saturated DMA/TFE (17:3, v/v) solution containing 1 μM **Co5**, 150 μM $Ir(ppy)_3$ and 0.1 M BIH under visible-light irradiation (225W Xe lamp equipped with 420 nm long pass filter and CM-1 cold mirror, wavelength $420 \leq \lambda \leq 750$ nm).

Conclusion

I have investigated the effect of metal ion substitution on the catalytic activity of multinuclear metal complexes. I have developed a novel pentanuclear metal complex that consists of five cobalt ions and six bpp^- ligands (**Co5**). **Co5** was easily synthesized by mixing a cobalt source and Hbpp ligand and was crystallographically characterized. Electrochemical measurements revealed that **Co5** exhibits multielectron reduction ability, making it completely distinct from **Fe5**, which shows multielectron oxidation ability. Moreover, the cyclic voltammetry of **Co5** under CO_2 indicates the catalytic activity of the complex for CO_2 reduction. Encouraged by these results, a photochemical reaction was conducted under CO_2 in a DMA/TFE solution containing **Co5** (catalyst), Ir(ppy)3 (photosensitizer), and BIH (sacrificial electron donor) with visible light irradiation. As a result, the photochemical CO_2 reduction proceeded successfully, and CO and HCOOH, which are two-electron reduced products of CO_2, were generated. The present results demonstrate that the use of multinuclear metal complexes is one of the strategies to develop novel catalysts for multielectron CO_2 reduction. Such insight should facilitate the development of a variety of multinuclear-metal-complex-based catalysts for small-molecule conversion.

Experimental section

Materials

$Co(CH_3COO)_2 \cdot 4H_2O$, $NaBF_4$, NaOH, $Ir(ppy)_3$, aqueous solutions of NaOH and HCl, and all the solvents except for *N,N*-dimethylacetamide (DMA) were purchased from FUJIFILM Wako Pure Chemical Corporation. 3,5-Bis(2-pyridyl)pyrazole, 2-phenylbenzimidazole, tetra-*n*-butylammonium perchlorate (TBAP), methyl iodide and DMA were purchased from Tokyo Chemical Industry Co., Ltd. $NaBH_4$ was purchased from Aldrich. $Zn(CH_3COO)_2 \cdot 2H_2O$ was purchased from Kanto Chemical Co., Inc. All the reagents were of highest quality available and were used as received except for TBAP. TBAP was recrystallized from absolute ethanol. H_2O was purified using a Millipore MilliQ purifier. 1,3-dimethyl-2-phenyl-2,3-dihydro-1*H*-benzo[d]imidazole (BIH) was synthesized using the slightly modified procedure reported in the literature.[39]

X-ray crystallography

Data collection for **Co5** was performed at 123 K on a ROD, Synergy Custom system (Rigaku Oxford Diffraction) equipped with confocal monochromated Mo-Kα radiation, and data were processed using CrysAlisPro 1.171.39.43c (Rigaku Oxford Diffraction). The structure was solved by direct methods using SIR-97 and refined by the full-matrix least squares techniques on F^2 (SHELXL-2014/3). All nonhydrogen atoms were refined anisotropically and refined with a riding model with U_{iso} constrained to be 1.2 times U_{eq} of the carrier atom. Crystallographic data have been deposited with Cambridge Crystallographic Data Centre: CCDC deposition number; 1949862 for $\mathbf{Co_5}(BF_4)_3$. Copies of the data can be obtained free of charge via www.ccdc.cam.ac.uk/data_request/cif.

Electrochemical studies

Cyclic voltammetry was performed with a Bio-Logic-Science Instruments potentiostat interfaced to a computer with SP-50 software, at room temperature under Ar or CO_2 using one compartment cell with a standard three-electrode configuration, which consisted of a glassy carbon disk (diameter 3 mm, from BAS Inc.), a Ag/Ag^+ couple, and a platinum wire as the working, reference, and auxiliary electrodes, respectively. The working electrode was treated between scans by means of polishing with 0.05 μm alumina paste (from BAS Inc.) and washing with purified H_2O. Ferrocene was used as an internal standard, and all potentials reported within this work are referenced to the ferrocenium/ferrocene couple at 0 V.

Assignment of redox peaks of Co5

Synthesis of $[Zn^{II}_5OH(bpp)_6](BF_4)_3$ (**Zn5**$(BF_4)_3$) was performed by modifying the procedure reported in the literatures.[52,53] Figure 11 was a cyclic voltammogram of **Zn5**. **Zn5** did not show any redox peaks in the potential region of 1.2 - −2.3 V.

The CVs of **Co5** and heterometallic pentanuclear metal complexes are shown in Figure 11.[51]

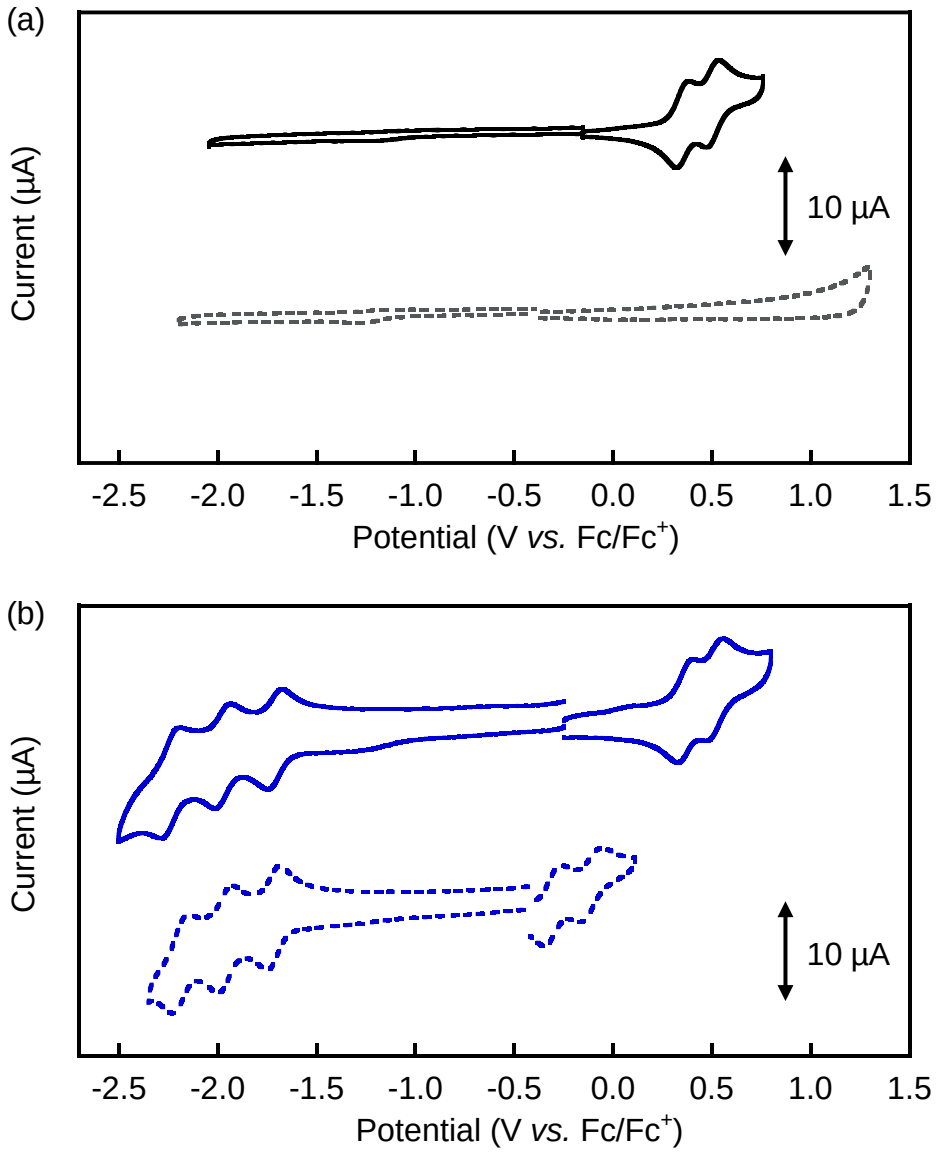

Figure 11. Cyclic voltammograms of a series of heterometallic (solid lines) and homometallic (dashed lines) pentanuclear metal complexes (0.2 mM) in acetonitrile solutions containing TBAP (0.1 M) at a scan rate of 100 mV/s; (a) **Ru2Zn3** and **Zn5** and (b) **Ru2Co3** and **Co5**.

Controlled-potential electrolysis (CPE)

CPE was performed in a gas-tight two-compartment electrochemical cell as in Figure 12. In the first compartment, the carbon plate working electrode and a leakless Ag/AgCl reference electrode (Innovative Instrument, Inc.) were immersed in 0.1 M TBAP/MeCN (5mL) containing 0.2 mM of **Co5** and 5 % trifluoroethanol. In the second compartment, the Pt auxiliary electrode was immersed in 0.1 M TBAP/MeCN (5 mL) containing ferrocene (40 mM) as a sacrificial reductant. The two compartments were separated by an anion exchange membrane (Selemion DSV). The solution was purged with CO_2 for 30 min prior to electrolysis. The electrolysis was performed for 1 h with constant stirring.

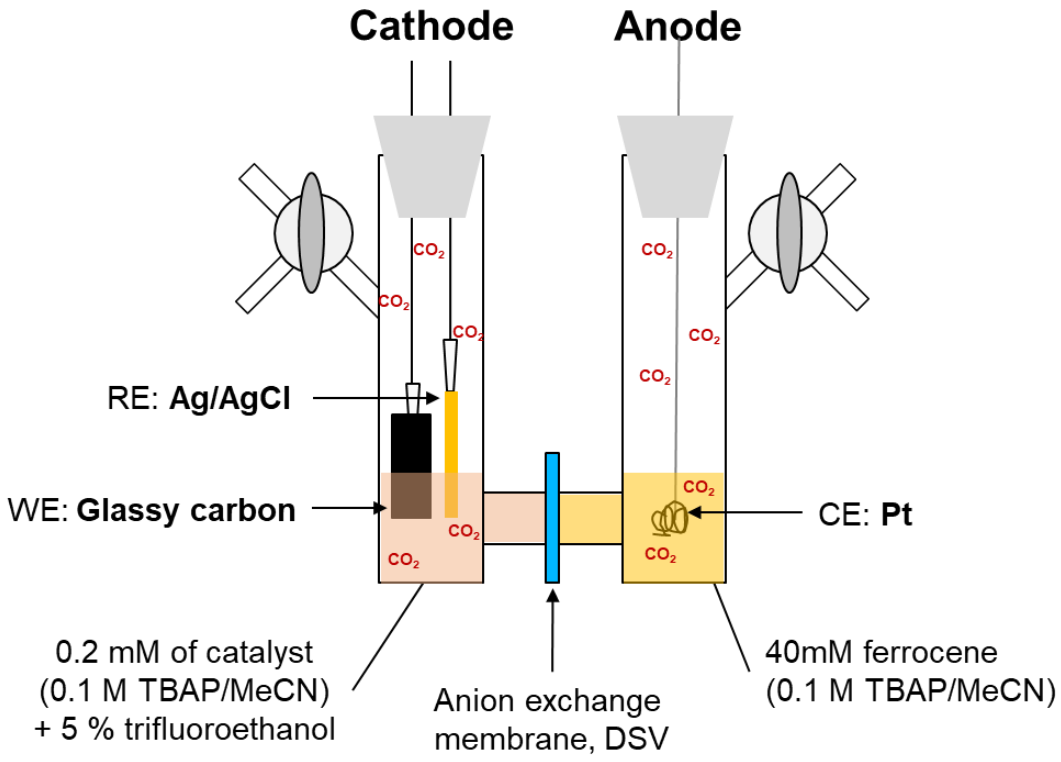

Figure12. General setup for controlled-potential electrolysis performed in this work.

Photochemical reaction

For a typical run, a mixed solution of DMA/TFE (17:3, v/v) (2.0 mL) containing 30 μM **Co5**, 150 μM $Ir(ppy)_3$ and 0.10 M BIH was purged with CO_2 for 15 minutes unless otherwise stated. The solution was then irradiated with a blue LED (wavelength λ = 420 nm) or xenon lamp (225W Xe lamp equipped with 420 nm long pass filter (Edmund Industrial Optics) and CM-1 cold mirror, wavelength $420 \leq \lambda \leq 750$ nm) at 20 °C in a custom made aluminium box with cooling system (Figure 13, 14). The amount of CO, H_2 and HCOOH produced in the reaction was quantified by GC and LC.

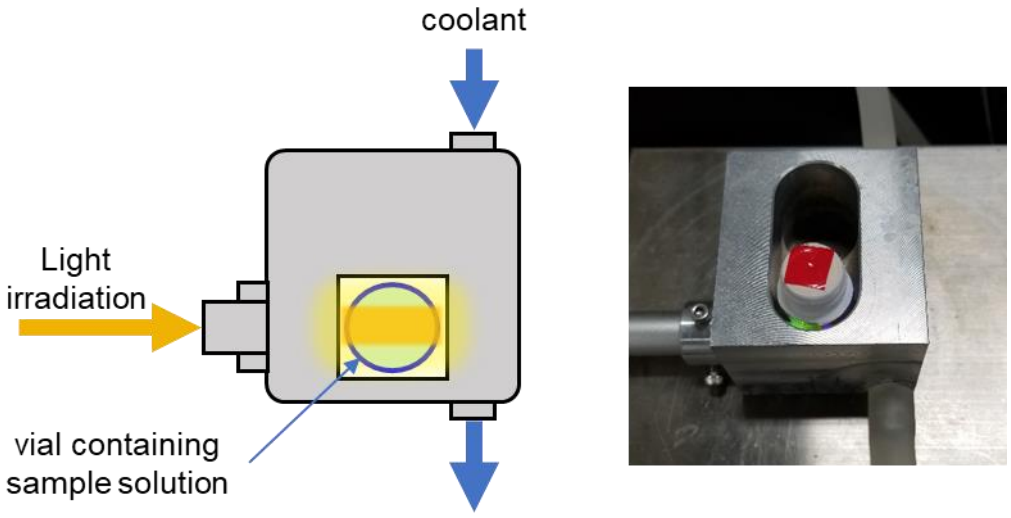

Figure 13. General setup for photochemical CO_2 reduction using blue LED carried out in this work.

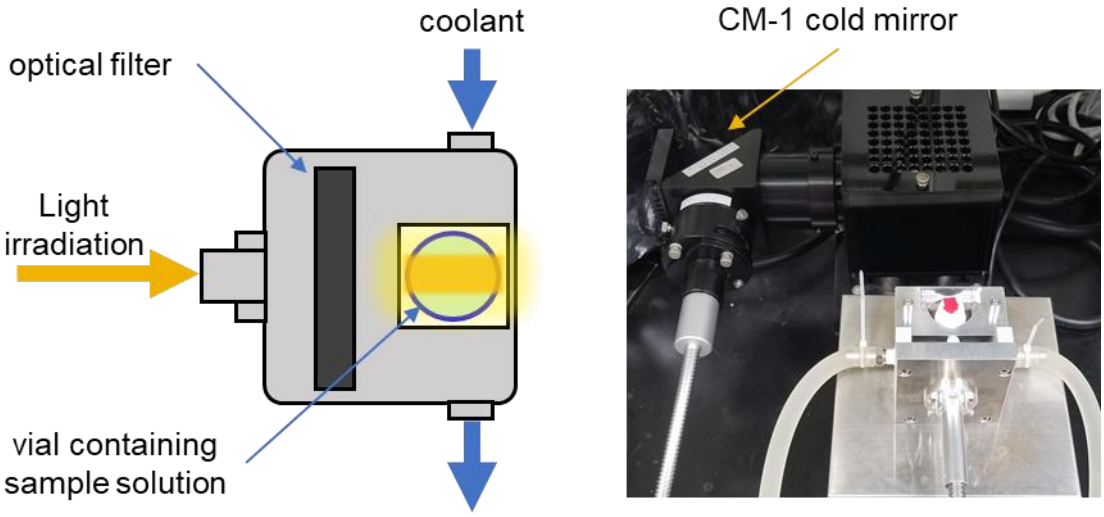

Figure 14. General setup for photochemical CO_2 reduction using xenon lamp and optical filter carried out in this work.

Product detection

The amount of CO and H_2 produced at the headspace of the cell was quantified by a Shimadzu GC-8A with a TCD detector equipped with a packed column with Molecular Sieve 13X-S 60/80 (He carrier gas, 40 °C) and a Shimadzu GC-2014 with a TCD detector equipped with a packed column with Molecular Sieve 5A (Ar carrier gas, 40 °C). Additionally, the liquid product was quantified by using a Shimadzu LC-20AD with SPD-20A and RID-10A detectors equipped with a Shim-pack SCR 102H column. Calibration curves were obtained by sampling known amounts of H_2, CO, and HCOOH.

$^{13}CO_2$ labeling experiment

A mixed solution of DMA/TFE (17:3, v/v) (2.0 mL) containing 30 μM **Co5**, 150 μM $Ir(ppy)_3$, and 0.10 M BIH was purged with Ar for 15 min, followed by $^{13}CO_2$ bubbling for 15 min. The $^{13}CO_2$ gas was produced by adding aqueous solution of HCl (2.0 M) to solid $Ba^{13}CO_3$ (98 atom % 13C, Sigma Aldrich) (Figure 15). The evolved CO was detected by a GCMS-QP2020 (Rt-Msieve 5A (30 m, 0.53 mm ID, 50 μm d_f) He carrier gas, 40 °C).

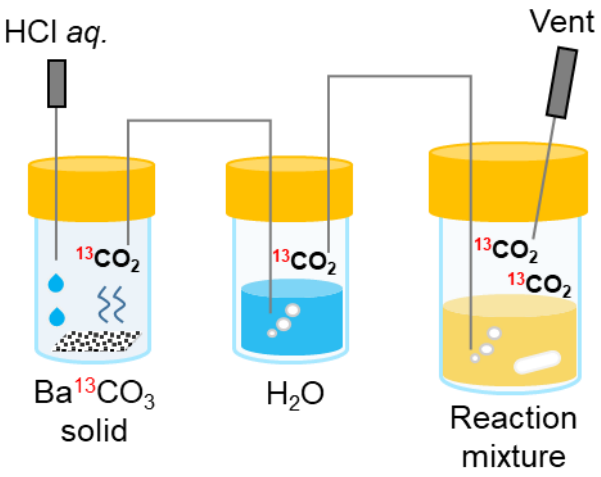

Figure 15. General setup for $^{13}CO_2$ labeling experiment.

Absorption spectrum of $Ir(ppy)_3$

The UV-Vis absorption spectrum of 30 μM $Ir(ppy)_3$ in acetonitrile was shown in Figure 16. $Ir(ppy)_3$ has a strong absorption band in the visible region.

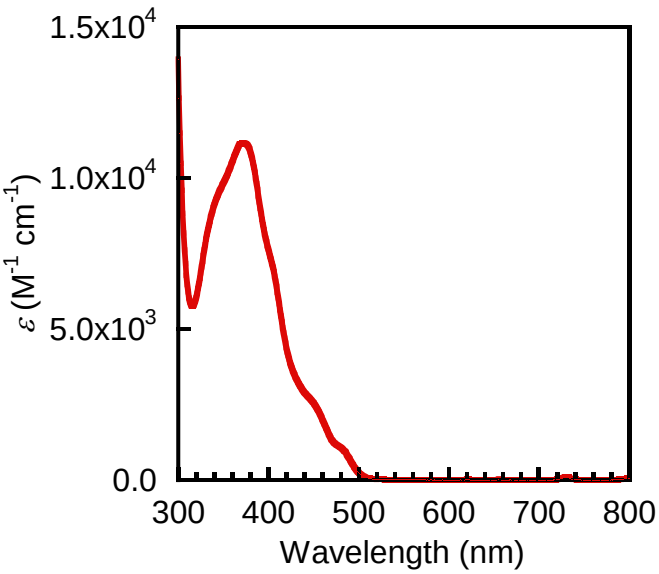

Figure 16. The absorption spectrum 30 μM $Ir(ppy)_3$ in acetonitrile. The spectrum was recorded on a UV-Vis Agilent Cary8454 spectrophotometer.

References

1. R. Chakrabarty, P. S. Mukherjee, P. J. Stang, Chem. Rev., 2011, 111, 6810.
2. J. Klingele, S. Dechert and F. Meyer, Coord. Chem. Rev., 2009, 253, 2698.
3. T. Shiga, G. N. Newton and H. Oshio, Dalton Trans., 2018, 47, 7384.
4. M. Venturi, A. Credi and V. Balzani, Coord. Chem. Rev., 1999, 185-186, 233.
5. M. Ruben, E. Breuning, J. -P. Gisselbrecht and J. -M. Lehn, Angew. Chem. Int. Ed., 2000, 39, 4139.
6. L. Arnold, C. J. Stevens, N. L. Bell, R. M. Lord, J. M. Goldberg, G. S. Nichol and J. B. Love, Chem. Sci., 2017, 8, 3609.
7. R. Sessoli, D. Gatteschi, A. Caneschi and M. A. Novak, Nature, 1993, 365, 141.
8. T. Matsumoto, G. N. Newton, T. Shiga, S. Hayami, Y. Matsui, H. Okamoto, R. Kumai, Y. Murakami and H. Oshio, Nat. Commun., 2014, 5, 3865.
9. P. C. Ford, E. Cariati and J. Bourassa, Chem. Rev., 1999, 99, 3625.
10. T. Morimoto, C. Nishiura, M. Tanaka, J. Rohacova, Y. Nakagawa, Y. Funada, K. Koike, Y, Yamamoto, S. Shishido, T. Kojima, T. Saeki, T. Ozeki and O. Ishitani, J. Am. Chem. Soc., 2013, 135, 13266.
11. Y. Tamaki, T. Morimoto, K. Koike and O. Ishitani, Proc. Natl. Acad. Sci. U.S.A., 2012, 109, 15673.
12. W. Ruettinger, M. Yagi, K. Wolf, S. Bernasek and G. C. Dismukes, J. Am. Chem. Soc., 2000, 122, 10353.
13. V. K. K. Praneeth, M. Kondo, M. Okamura, T. Akai, H. Izu and S. Masaoka, Chem. Sci., 2019, 10, 4628.
14. M. Yagi, M. Toda, S. Yamada and H. Yamazaki, Chem. Commun., 2010, 46, 8594.
15. Y. Umena, K. Kawakami, J. -R. Shen and N. Kamiya, Nature, 2011, 473, 55.
16. M. Suga, F. Akita, M. Sugahara, M. Kubo, Y. Nakajima, T. Nakane, K. Yamashita, Y. Umena, M. Nakabayashi, T. Yamane, T. Nakano, M. Suzuki, T. Masuda, S. Inoue, T. Kimura, T. Nomura, S. Yonekura, L. -J. Yu, T. Sakamoto, T. Motomura, J. -H. Chen, Y. Kato, T. Noguchi, K. Tono, Y. Joti, T. Kameshima, T. Hatsui, E. Nango, R. Tanaka, H. Naitow, Y. Matsuura, A. Yamashita, M. Yamamoto, O. Nureki, M. Yabashi, T. Ishikawa, S. Iwata and J. -R. Shen, Nature, 2017, 543, 131.
17. M. M. Georgiadis, H. Komiya, P. Chakrabarti, D. Woo, J. J. Kornuc and D. C. Rees, Science, 1992, 257, 1653.

18. J. Kim and D. C. Rees, Science, 1992, 257, 1677.
19. B. M. Hoffman, D. Lukoyanov, Z. -Y. Yang, D. R. Dean and L. C. Seefeldt, Chem. Rev., 2014, 114, 4041.
20. T. I. Doukov, T. M. Iverson, J. Seravalli, S. W. Ragsdale and C. L. Drennan, Science, 2002, 298, 567.
21. J. -H. Jeoung and H. Dobbek, Science, 2007, 318, 1461.
22. M. Okamura, M. Kondo, R. Kuga, Y. Kurashige, T. Yanai, S. Hayami, V. K. K. Praneeth, M. Yoshida, K. Yoneda, S. Kawata and S. Masaoka, Nature, 2016, 530, 465.
23. J. Hawecker, J. -M. Lehn and R. Ziessel, J. Chem. Soc. Chem. Commun., 1983, 536.
24. H. Takeda, K. Koike, H. Inoue and O. Ishitani, J. Am. Chem. Soc., 2008, 130, 2023.
25. H. Ishida, T. Terada, K. Tanaka and T. Tanaka, Inorg. Chem., 1990, 29, 905.
26. Y. Kuramochi, M. Kamiya and H. Ishida, Inorg. Chem., 2014, 53, 3326.
27. K. Kobayashi, T. Kikuchi, S. Kitagawa and K. Tanaka, Angew. Chem. Int. Ed., 2014, 53, 11813.
28. H. Rao, L. C. Schmidt, J. Bonin and M. Robert, Nature, 2017, 548, 74.
29. S. Matsuoka, K. Yamamoto, T. Ogata, M. Kusaba, N. Nakashima, E. Fujita and S. Yanagida, J. Am. Chem. Soc., 1993, 115, 601.
30. L. Chen, Z. Guo, X. -G. Wei, C. Gallenkamp, J. Bonin, E. Anxolabéhère-Mallart, K. -C. Lau, T. -C. Lau and M. Robert, J. Am. Chem. Soc., 2015, 137, 10918.
31. S. L. -F. Chan, T. L. Lam, C. Yang, S. -C. Yan and N. M. Cheng, Chem. Commun., 2015, 51, 7799.
32. F. Wang, B. Cao, W. -P. To, C. -W. Tse, K. Li, X. -Y. Chang, C. Zang, S. L. -F. Chan and C. -M. Che, Catal. Sci. Technol., 2016, 6, 7408.
33. Z. Guo, S. Cheng, C. Cometto, E. Anxolabéhère-Mallart, S. M. Ng, C. -C. Ko, G. Liu, L. Chen, M. Robert and T. -C. Lau, J. Am. Chem. Soc., 2016, 138, 9413.
34. T. Ouyang, C. Hou, J. -W. Wang, W. -J. Liu, D. -C. Zhong, Z. -F. Ke and T. -B. Lu, Inorg. Chem., 2017, 56, 7307.
35. T. Shimoda, T. Morishima, K. Kodama, T. Hirose, D. E. Polyansky, G. F. Manbeck, J. T. Muckerman and E. Fujita, Inorg. Chem., 2018, 57, 5486.
36. D. -C. Liu, H. -H. Huang, J. -W. Wang, L. Jiang, D. -C. Zhong and T. -B. Lu, ChemCatChem, 2018, 10, 3435.
37. J. -W. Wang, H. -H. Huang, J. -K. Sun, T. Ouyang, D. -C. Zhong and T. -B. Lu,

ChemSusChem, 2018, 11, 1025.
38. A. Call, M. Cibian, K. Yamamoto, T. Nakazono, K. Yamauchi and K. Sakai, ACS Catal., 2019, 9, 4867.
39. D. Hong, Y. Tsukakoshi, H. Kotani, T. Ishizuka and T. Kojima, J. Am. Chem. Soc., 2017, 139, 6538.
40. H. Shirley, X. Su, H. Sanjanwala, K. Talukdar, J. W. Jurss and J. H. Delcamp, J. Am. Chem. Soc., 2019, 141, 6617.
41. E. Fujita, Coord. Chem. Rev., 1999. 185-186, 373.
42. Y. Yamazaki, H. Takeda and O. Ishitani, J. Photochem. Photobiol. C: Photochem. Rev., 2015, 25, 106.
43. H. Takeda, C. Cometto, O. Ishitani and M. Robert, ACS Catal., 2017, 7, 70.
44. Y. Kuramochi, O. Ishitani and H. Ishida, Coord. Chem. Rev., 2018, 373, 333.
45. T. Ouyang, H. -H. Huang, J. -W. Wang, D. -C. Zhong and T. -B. Lu, Angew. Chem. Int. Ed., 2017, 56, 738.
46. L. -M. Cao, H. -H. Huang, J. -W. Wang, D. -C. Zhong and T. -B. Lu, Green Chem., 2018, 20, 798.
47. J. -W. Wang, D. -C. Zhong and T. -B. Lu, Coord. Chem. Rev., 2018, 377, 225.
48. M. D. Rail, L. A. Berben, J. Am. Chem. Soc., 2011, 133, 18577.
49. D. B. Cluff, A. Arnold, J. C. Fettinger, L. A. Berben, Organometallics, 2019, 38, 1230.
50. D. J. Szalda, C. Creutz, D. Mahajan and N. Sutin, Inorg. Chem., 1983, 22, 2372.
51. H. Izu, M. Kondo, M. Okamura, M. Tomoda, S. K. Lee, T. Akai, V. K. K. Praneeth, M. Kanaike, S. Kawata and S. Masaoka, ChemRxiv Preprint, DOI: 10.33774/chemrxiv-2021-n3jtl.
52. J. -Z. Hou, M. Li, Z. Li, S. -Z. Zhan, X. -C. Huang and D. Li, Angew. Chem. Int. Ed., 2008, 47, 1711.
53. S. Romain, J. Rich, C. Sens, T. Stoll, J. Benet-Buchholz, A. Llobet, M. Rodriguez, I. Romero, R. Clérac, C. Mathonière, C. Duboc, A. Deronzier and M. -N. Collomb, Inorg. Chem., 2011, 50, 8427.

Chapter 2

Photochemical hydrogen production based on CO2/HCOOH cycle promoted by pentanuclear cobalt complex

Introduction

With the increasing demand for energy and the rapid depletion of fossil fuels, the development of renewable and environmentally friendly energy sources has become essential. In this respect, hydrogen gas is a promising energy carrier and a clean alternative to conventional fossil fuels. However, its gaseous nature and low volumetric energy density make it difficult to store and transport. Given this background, significant research efforts have focused on the liquid organic hydrogen carrier HCOOH, which is a low-toxicity liquid under ambient conditions.[1-3] Its ease of storage and transportation and high volumetric energy density make it a viable hydrogen carrier. Therefore, efficient catalysts for the production of HCOOH and its conversion into hydrogen are required for the utilization of HCOOH as a hydrogen carrier.

Catalysts that promote the release of hydrogen via the dehydrogenation of HCOOH have been studied extensively.[1-18] In this catalytic reaction, HCOOH is converted into molecular hydrogen and CO_2 ($HCOOH \rightarrow H_2 + CO_2$). By recycling the formed CO_2 back into HCOOH, a carbon-neutral cycle can be realized (Figure 1). To date, several catalysts that allow for reversible dehydrogenation/hydrogenation ($CO_2 + H_2 \rightarrow HCOOH$) between HCOOH and CO_2 (Figure 1(a)) have been reported.[1,19-23] Nevertheless, this cycling process involves the utilization of gaseous hydrogen and generally harsh reaction conditions (high pressure and/or heating)[19-25] for storing the hydrogen in the form of HCOOH (hydrogenation process). Another method for obtaining HCOOH from CO_2 is the two-electron reduction of CO_2 in the presence of protons ($CO_2 + 2H^+ + 2e^- \rightarrow HCOOH$). There have been a number of reports on catalysts that promote the photo- and electrochemical reduction of CO_2 into HCOOH under ambient conditions.[26-29] However, there are no reports on catalysts that can promote both the reduction of CO_2 and the dehydrogenation of HCOOH (Figure 1(b)).

In this chapter, I report the first example of a catalyst that shows catalytic activity for both the reduction of CO_2 and the dehydrogenation of HCOOH. A pentanuclear cobalt complex **Co5** can catalyze the photochemical reduction of CO_2 to produce HCOOH, was found to also catalyze the photoinduced dehydrogenation of HCOOH at ambient temperature. Under the optimized conditions, the turnover frequency (TOF) of **Co5** for the dehydrogenation reaction of HCOOH was higher (229 h^{-1}) than those reported for

other molecular catalysts that operate under photoirradiation at ambient temperature. In addition, mechanistic studies were performed to elucidate the underlying mechanism of the catalytic cycle, and the critical role of the Co^{I} species of **Co5** both in the HCOOH dehydrogenation reaction and the CO_2 reduction process was clarified. The results of this study should aid the development of new carbon-neutral energy cycles that use HCOOH as a hydrogen carrier.

Our study begins with a serendipitous finding upon examining the photocatalytic activity of **Co5** for CO_2 reduction. During this experiment, the photoirradiation of a solution containing **Co5**, a photosensitizer, a proton source, and a sacrificial electron donor in a CO_2 atmosphere resulted in the formation of HCOOH, CO, and H_2 (Chapter 1). Surprisingly, the evolution of hydrogen was completely suppressed in an Ar atmosphere, indicating that CO_2 is required for the generation of hydrogen. Given this observation, I assumed that the evolution of hydrogen originates from the dehydrogenation of HCOOH and not proton reduction.

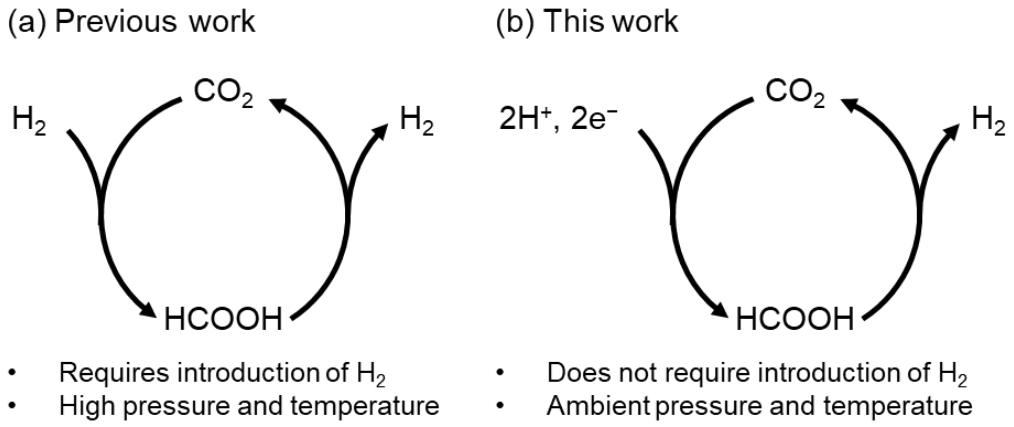

Figure 1. Two distinct CO_2/HCOOH cycles that use HCOOH as hydrogen carrier. (a) CO_2 hydrogenation and HCOOH dehydrogenation couple. (b) CO_2 reduction and HCOOH dehydrogenation couple.

Results and discussions

Photochemical formic acid dehydrogenation

Encouraged by the aforementioned result, I investigated the suitability of **Co5** as a catalyst for the dehydrogenation of HCOOH under photoirradiation. The initial reaction was performed in 2 mL of an DMA solution containing **Co5** (30 μM) as the catalyst, $Ir(ppy)_3$ (150 μM) as the photosensitizer, BIH (0.1 M) as the sacrificial electron donor, and HCOOH (500 *eq. versus* **Co5**) as the substrate in an Ar atmosphere under irradiation with visible light (blue LED, wavelength λ = 420 nm) at 20 °C. As shown in Figure 2, the evolution of hydrogen gas was observed after 3 h of photoirradiation. This result implies that **Co5** can catalyze the photoinduced dehydrogenation of HCOOH at ambient temperature.

A series of control experiments were performed to further investigate the catalytic reaction. First, a reaction was performed using trifluoroacetic acid (TFA) instead of HCOOH as a substrate. Only a small amount of hydrogen was detected (Table 1, No. 2), confirming that proton reduction cannot proceed under these conditions. In addition, reactions in the absence of **Co5**, $Ir(ppy)_3$, BIH, or light irradiation yielded hydrogen in trace amounts (Figure 2 and Table 1). Therefore, all the above-mentioned components are required to promote the dehydrogenation of HCOOH. These facts confirmed that **Co5** is suitable for use as a catalyst for the photochemical dehydrogenation of HCOOH at ambient temperature. Note that this is one of the few instances of the dehydrogenation of HCOOH under photoirradiation.[11-17]

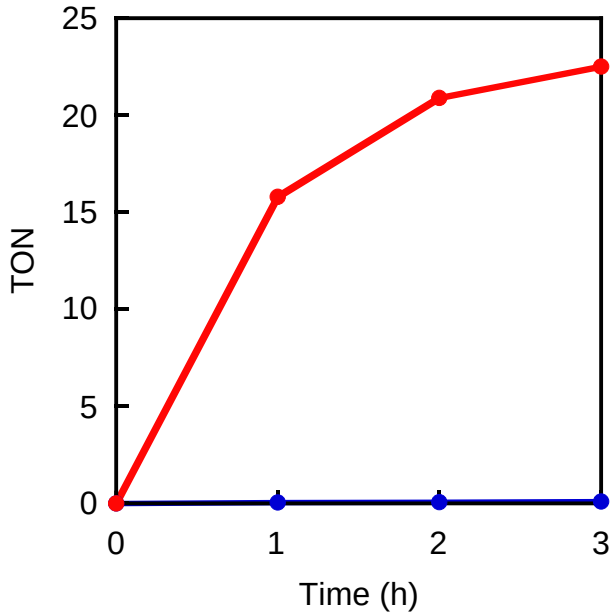

Figure 2. Photochemical production of H_2 in the presence of 30 μM **Co5** (red line) and in the absence of **Co5** (blue line) in Ar-saturated DMA solution containing 150 μM $Ir(ppy)_3$, 100 mM BIH, and 13 mM HCOOH at 20 °C.

Table 1. Control experiments for photocatalytic formic acid dehydrogenation reaction by **Co5**.[a]

No.	[**Co5**] (μM)	[$Ir(ppy)_3$] (μM)	[BIH] (M)	substrate	Light (nm)	TON_{H2}
1	30	150	0.1	HCOOH	420	22
2	30	150	0.1	TFA[b]	420	0.03
3	-	150	0.1	HCOOH	420	trace
4	30	-	0.1	HCOOH	420	0
5	30	150	-	HCOOH	420	0
6	30	150	0.1	HCOOH	dark	trace

[a] All experiments were carried out in DMA solution at 20 °C.

[b] TFA = trifluoroacetic acid.

The effect of photosensitizers on the catalytic performance

The dehydrogenation reactions were performed using different photosensitizers (Figure 3, 4), namely, $Ir(ppy)_3$, $[Ir(dtbbpy)(ppy)_2](PF_6)$ (**Ir-2**, dtbbpy = 4,4'-di-*t*-butyl-2,2'-bipyridine), and $[Ir(dF(CF_3)ppy)_2(dtbbpy)](PF_6)$ (**Ir-3**, $dF(CF_3)ppy$ = 2-(2,4-difluorophenyl)-5-(trifluoromethyl) pyridine). The reactions that used $Ir(ppy)_3$ and **Ir-2** as the photosensitizer resulted in the formation of hydrogen, whereas no hydrogen was detected when **Ir-3** was used (Figure 4). Of the three photosensitizers tested, $Ir(ppy)_3$ exhibited the highest efficiency for the dehydrogenation of HCOOH. Thus, I employed the complex as the photosensitizer for the subsequent investigations.

Based on these results, I was able to gain additional insights into the reaction mechanism. The choice of the photosensitizer greatly affects the efficiency of the system. This result can be explained based on the reduction potentials. The first reduction potentials, $E_{1/2}(Ir^{III}/Ir^{II})$, of the investigated photosensitizers are −2.64 ($Ir(ppy)_3$), −1.87 (**Ir-2**), and −1.74 V (**Ir-3**) (*vs.* Fc/Fc^+, Table 2). As examined in Chapter 1, **Co5** exhibits a one-electron reduction wave at $E_{1/2}(Co^{II}{}_5/Co^{II}{}_4Co^{I}) = -1.72$ V (*vs.* Fc/Fc^+), which is attributable to the reduction of the cobalt center at the triangular core (details of the assignment of redox peaks are also described in Chapter 1). A comparison of the redox potentials of the investigated photosensitizers and **Co5** revealed that $Ir(ppy)_3$ and **Ir-2** were able to reduce **Co5** during the photocatalytic reaction while **Ir-3** was difficult to reduce. As mentioned earlier, the reactions involving $Ir(ppy)_3$ and **Ir-2** resulted in hydrogen production, whereas that that used **Ir-3** as the photosensitizer did not. These results indicate that the one-electron-reduced species of **Co5** was involved in the reaction.

To confirm this hypothesis, CV was performed in the presence of **Co5** and HCOOH. The current at the first reduction peak of **Co5** was slightly higher compared with that in the absence of HCOOH (Figure 5). It should also be noted that this current enhancement was not observed when TFA was added to the solution (Figure 6). Thus, the cyclic voltammograms indicated that specific interactions occur between the one-electron reduced species of **Co5** and HCOOH. Therefore, the Co^I present at the triangular core plays a critical role in the reaction. This conclusion is consistent with the fact that all the previous examples of HCOOH dehydrogenation reactions mediated by cobalt complexes were triggered by the Co^I species.[9-11]

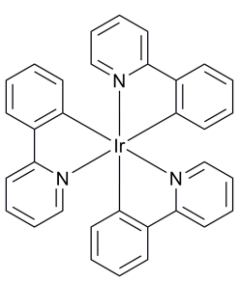

$Ir(ppy)_3$

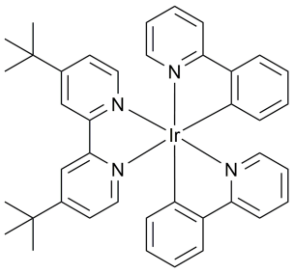

$[Ir(dtbbpy)(ppy)_2](PF_6)$

Ir-2

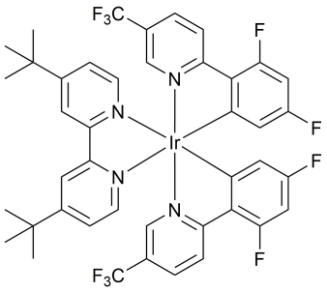

$[Ir(dF(CF_3)ppy)_2(dtbbpy)](PF_6)$

Ir-3

Figure 3. Structures of Ir photosensitizers.

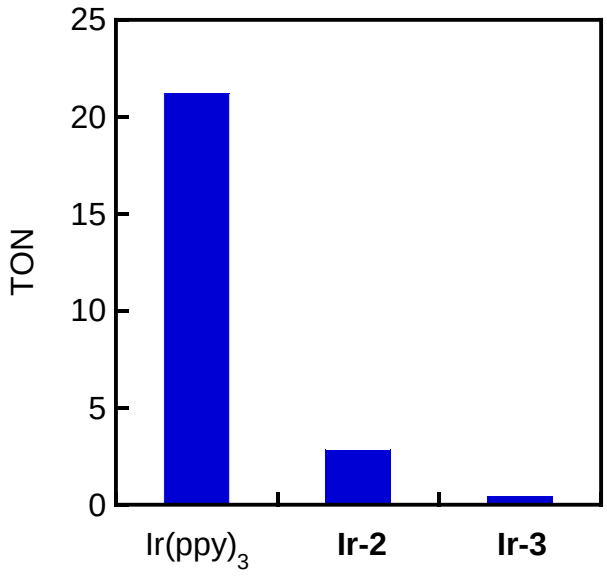

Figure 4. Photochemical HCOOH dehydrogenation activities of different photosensitizers: $Ir(ppy)_3$, **Ir-2**, and **Ir-3**. Reactions were performed in DMA solution containing 30 μM **Co5**, 150 μM photosensitizer, 100 mM BIH, and 13 mM HCOOH.

Table 2. First reduction potentials of $Ir(ppy)_3$, **Ir-2**, and **Ir-3**.

Photosensitizer	$Ir(ppy)_3$	**Ir-2**	**Ir-3**
$E_{1/2}(Ir^{III}/Ir^{II})$ (V *vs.* Fc/Fc^+)[a]	−2.64	−1.87	−1.74

[a]$E_{1/2}(Ir^{III}/Ir^{II})$ was determined from the results of cyclic voltammetry (CV). Standard conditions: 0.2 mM solutions of Ir complex under Ar in MeCN containing 0.1 M TBAP.

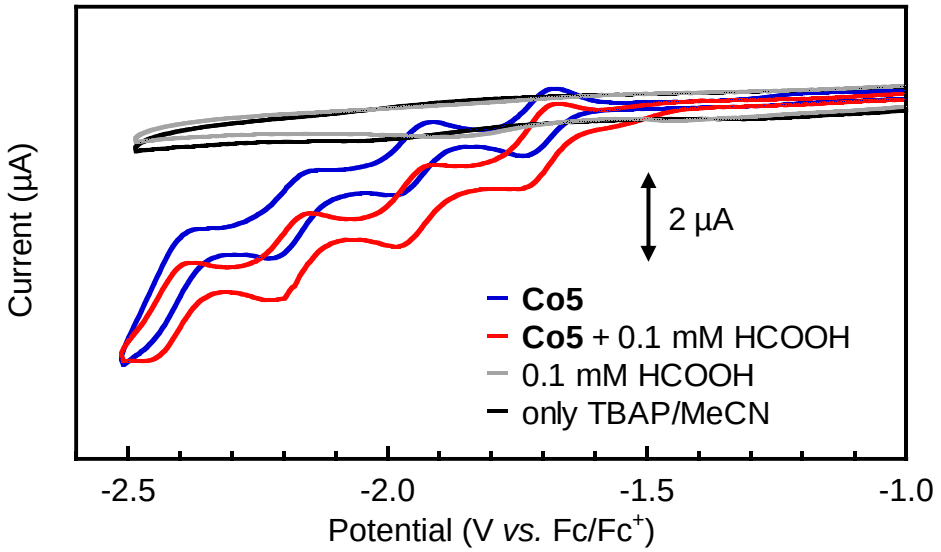

Figure 5. Cyclic voltammograms of 0.2 mM solution of **Co5** in the presence (red line) and in the absence (blue line) of 0.5 *eq.* HCOOH in acetonitrile containing 0.1 M TBAP. The CVs were measured using a GC electrode at a scan rate of 10 mV s^{-1}.

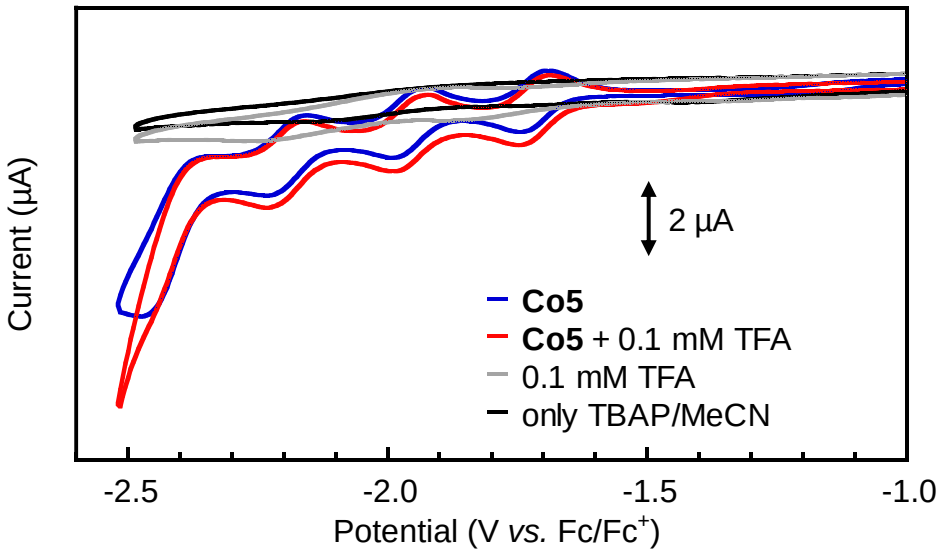

Figure 6. Cyclic voltammograms of 0.2 mM solution of **Co5** in the presence (red line) and in the absence (blue line) of 0.5 *eq.* TFA in acetonitrile containing 0.1 M TBAP. The CVs were measured using a GC electrode at a scan rate of 10 mV s^{-1}.

Next, the effect of the concentration of the photosensitizer, that is, $Ir(ppy)_3$, was investigated. The evolution of hydrogen accelerated with an increase in the concentration of $Ir(ppy)_3$ (Figure 7), suggesting that the dehydrogenation of HCOOH in the proposed system occurred readily at higher $Ir(ppy)_3$ concentrations.

As mentioned before, the formation of Co^I at the triangular core via the photoinduced one-electron reduction of **Co5** is essential for the reaction. Therefore, it was expected that an increase in the concentration of $Ir(ppy)_3$ would increase the rate of photoinduced electron transfer. In other words, the concentration of $Ir(ppy)_3$ has a determining effect on the frequency of the photoinduced electron transfer events. Note that the concentrations of $Ir(ppy)_3$ employed in our photocatalytic investigations are low enough that all the incident photons were not absorbed; the fraction of light absorbed during the photocatalytic experiment is in the range from 53 % to 98%.

That CO_2 is also formed during the catalysis process was confirmed using gas chromatography (Figure 7).

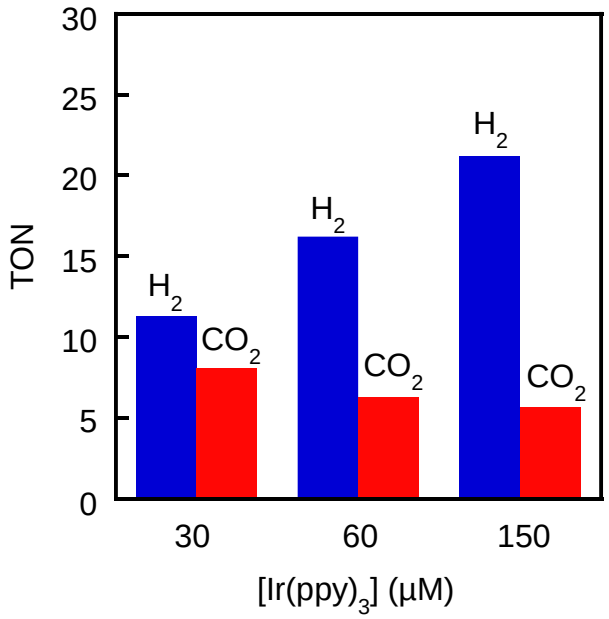

Figure 7. Effect of $Ir(ppy)_3$ concentration on H_2 (blue bar) and CO_2 (red bar) production by HCOOH dehydrogenation. Reactions were performed in DMA solution containing 30 μM **Co5**, 30-150 μM $Ir(ppy)_3$, 100 mM BIH, and 13 mM HCOOH.

The effect of BIH on the catalytic performance

Finally, the effect of the concentration of the sacrificial electron donor (BIH) was investigated. As shown in Figure 8, as the concentration of BIH was increased, the amount of hydrogen generated decreased dramatically, indicating that the presence of BIH in a higher concentration hindered the dehydrogenation reaction.

The effect of the concentration of BIH on the catalysis process can be understood based on the photoinduced electron transfer pathway for the formation of the key intermediate, namely, the one-electron reduced species of **Co5** with Co^{I} at the triangular core. As described in Chapter 1, there are two possible pathways: the oxidative quenching and reductive quenching for accessing this species. I have revealed that emission quenching was observed upon increasing the concentration of **Co5**/BIH in a solution of $Ir(ppy)_3$. The corresponding quenching rate constants for the oxidative and reductive quenching pathways were determined to be k_q = 6.6 x 10^9 and 5.5 x 10^6 M^{-1} s^{-1}, respectively. Considering that the concentration of BIH is approximately 10^3 times higher than that of **Co5** in the proposed photocatalytic reaction, the rates of the two quenching pathways are comparable. At a BIH concentration of 50 mM, the calculated oxidative and reductive quenching rates are almost identical. In addition, the experimental results showed clearly that the catalysis reaction is deaccelerated when BIH is added in a higher concentration (Figure 8). Oxidative quenching was dominant at lower BIH concentrations whereas reductive quenching was dominant at higher concentrations. Therefore, it can be concluded that the photochemical dehydrogenation of HCOOH using the proposed system occurs readily when oxidative quenching is dominant. It should be noted that the formation of HBIH cation via the reaction between BIH and HCOOH can also deaccelerate the catalysis as the concentration of protons to react with the postulated hydride intermediate (*vide infra*) decreases to some extent.

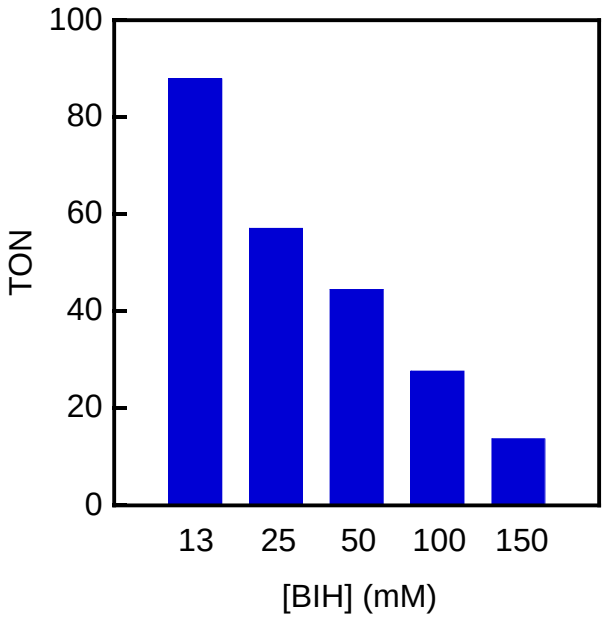

Figure 8. Effect of BIH concentration for HCOOH dehydrogenation. Reactions were performed in DMA solution containing 30 μM **Co5**, 150 μM $Ir(ppy)_3$, 25-150 mM BIH, and 13 mM HCOOH.

Possible mechanism

Based on the results described above as well as those of previous reports on the dehydrogenation of HCOOH, a possible mechanism for the described catalytic system based on **Co5** is proposed (Scheme 1). First, a single cobalt ion in the triangular core of **Co5**, which exhibits a pentacoordinated structure, is reduced by $Ir(ppy)_3$ through oxidative quenching. Based on the experimental results, including the dependence of the catalytic performance of **Co5** on the choice of the photosensitizer (Figure 4) and the CV measurements of **Co5** performed in the presence of HCOOH (Figure 5), it can be concluded that the one-electron reduced species of **Co5** is the key active species in the reaction. This one-electron reduced species reacts with HCOOH and releases hydrogen and CO_2 (HCOOH dehydrogenation). That CO_2 is formed during the catalysis process was confirmed using gas chromatography (Figure 7). In this process, it is assumed that Co^I promotes the elimination of the C-H bond, like other cobalt complexes that catalyze HCOOH dehydrogenation reactions.[9-11] Moreover, it has been reported that the synergistic effects between the distinct metal ions play an important role in the dehydrogenation reaction.[17,18,30] Thus, the multinuclear metal structure of **Co5** is an effective one for catalysis.

In addition to participating in the HCOOH dehydrogenation reaction, the one-electron reduced species of **Co5** also reacts with the CO_2 generated during the dehydrogenation reaction. The species receives a single electron from the photosensitizer and reduces CO_2 to HCOOH or CO (CO_2 reduction process). This CO_2 reduction process requires the injection of one more electron into the catalyst. To be able to access this two-electron-reduced species, electron transfer from the photosensitizer to **Co5** is necessary. Therefore, it can be assumed that the CO_2 reduction reaction will be accelerated under conditions where photoinduced electron transfer events occur frequently. As mentioned above, the concentration of $Ir(ppy)_3$ can be used to control the frequency of the photoinduced electron transfer events. Indeed, the amount of CO_2 detected depended primarily on the concentration of $Ir(ppy)_3$. On increasing the concentration of $Ir(ppy)_3$, the amount of CO_2 detected decreased (Figure 7), even though the amount of hydrogen generated by the dehydrogenation of HCOOH increased. This might indicate that the CO_2 formed by the dehydrogenation of HCOOH was consumed by the CO_2 reduction process. Thus, the dual catalysis mechanism explains both the dehydrogenation of HCOOH and the two-electron reduction of CO_2 mediated by **Co5**. This demonstrates the construction of an unconventional CO_2/HCOOH cycle.

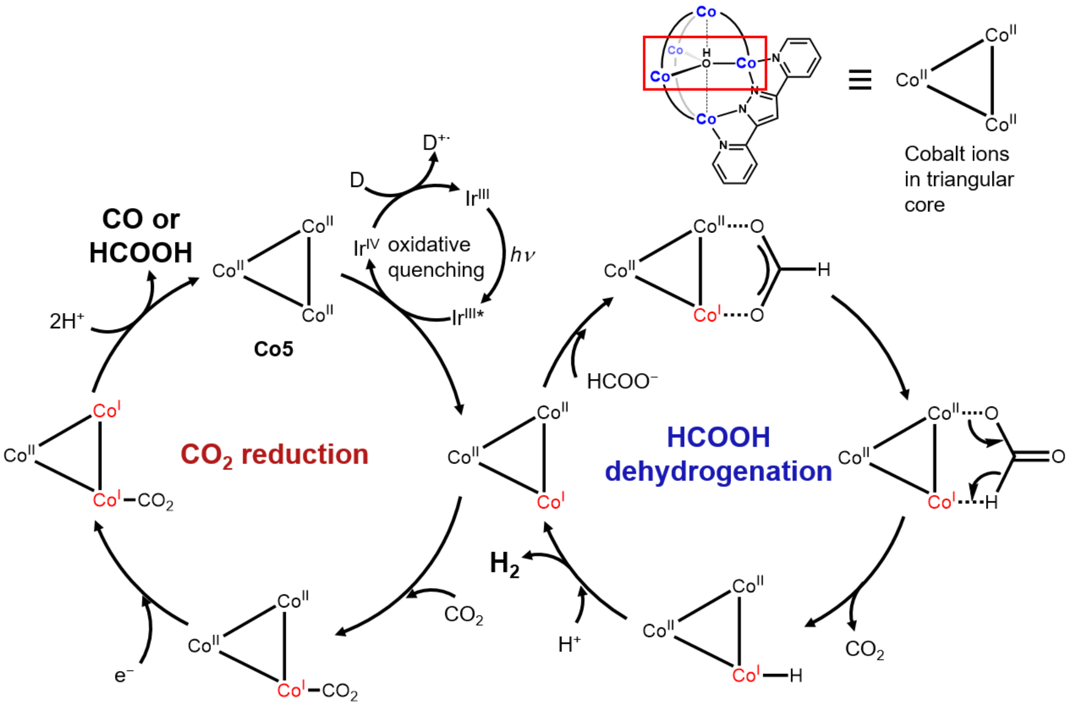

Scheme 1. Proposed mechanism of the dual catalysis process mediated by **Co5**. Dehydrogenation of HCOOH (right) and two-electron reduction of CO_2 (left).

Optimization

Finally, I optimized the reaction conditions for the HCOOH dehydrogenation reaction. By decreasing the concentration of BIH to 25 mM and increasing that of HCOOH to 25 mM and performing photoirradiation with an Xe lamp ($420 < \lambda < 750$ nm), the maximum turnover number for the reaction could be increased to 229 after 1 h (Table 3). The turnover frequency (TOF, 229 h^{-1}) under this condition is the highest observed for molecular catalysts that operate under photoirradiation at ambient temperature (Table 3 and Figure 9).

Table 3. Comparison of catalytic activity of the relevant catalysts for photochemical formic acid dehydrogenation.

catalyst	Concentration	Temp. (°C)	TON (time)	TOF (h^{-1})[a]	Ref.
Co5	0.03 mM	r.t.	229 (1 h)	229	This work
$[CoH\{PPh(OEt)_2\}_4]$	20 mM	30	3.06 (6 h)	0.51	11
$Fe_3(CO)_{12}/PPh_3$/tpy	3 mM	25	8.1 (3h)	2.7	14
$Fe_3(CO)_{12}/PPh_3$/phen	3 mM	60	126 (24h)	5.2	14
$Ir_2H_5(xylBINAP)_2(BF_4)$ (**4**)	3 mol%	r.t.	280 (24 h)	12	17
[Cp*Ir(bpy-OMe)(Cl)](Cl) (**5**)	0.37 mM	r.t.	~500 (30 h)	~17	15

[a] The turnover frequency (TOF, h^{-1}) was calculated by dividing the turnover number (TON) with duration of photoirradiation.

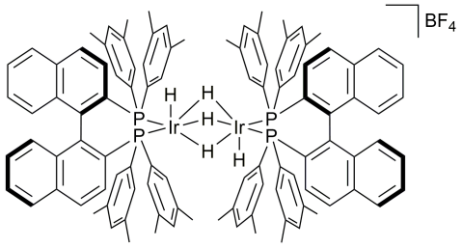

4

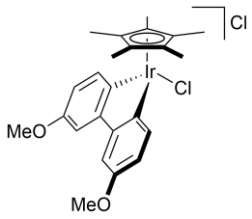

5

Figure 9. Molecular structures of photocatalysts for formic acid dehydrogenation (**4** and **5**) shown in Table 3.

Conclusion

I have revealed the catalytic activity of a pentanuclear cobalt complex (**Co5**) for the photoinduced dehydrogenation of HCOOH. The dehydrogenation reactions were performed under photoirradiation in the presence of **Co5**, a suitable photosensitizer, and sacrificial electron donor at ambient temperature and resulted in the generation of H_2 and CO_2. This is a rare example of the photoinduced dehydrogenation of HCOOH under ambient conditions. In addition, it was determined that the activity of **Co5** is higher than those of similar previously reported molecular catalysts. Mechanistic investigations indicated that the one-electron-reduced species of **Co5** plays an essential role in the catalytic cycle. Given that **Co5** also catalyzes the photochemical two-electron reduction of CO_2 into HCOOH, this study is the first example of a hydrogen storage/release cycle based on the photochemical reduction of CO_2 and dehydrogenation of HCOOH.

Experimental section

Materials

$Ir(ppy)_3$, formic acid, trifluoroacetic acid, and all the solvents except for *N,N*-dimethylacetamide (DMA) were purchased from FUJIFILM Wako Pure Chemical Corporation. Tetra-*n*-butylammonium perchlorate (TBAP), and DMA were purchased from Tokyo Chemical Industry Co., Ltd. $[Ir(dtbbpy)(ppy)_2](PF_6)$ and $[Ir(dF(CF_3)ppy)_2(dtbbpy)](PF_6)$ was purchased from Aldrich. All the reagents were of highest quality available and were used as received except for TBAP. TBAP was recrystallised from absolute ethanol. H_2O was purified using a Millipore MilliQ purifier.

Electrochemical studies

Cyclic voltammetry was performed with a Bio-Logic-Science Instruments potentiostat interfaced to a computer with SP-50 software, at room temperature under Ar using one compartment cell with a standard three-electrode configuration, which consisted of a glassy carbon disk (diameter 3 mm, from BAS Inc.), a Ag/Ag^+ couple, and a platinum wire as the working, reference, and auxiliary electrodes, respectively. The working electrode was treated between scans by means of polishing with 0.05 μm alumina paste (from BAS Inc.) and washing with purified H_2O. Ferrocene was used as an internal standard, and all potentials reported within this work are referenced to the ferrocenium/ferrocene couple at 0 V.

Photochemical reaction

For a typical run, a mixed solution of DMA (2.0 mL) containing 30 μM **Co5**, 150 μM $Ir(ppy)_3$ and 0.10 M BIH, and HCOOH (13 mM, 500 *eq. vs.* **Co5**) was purged with Ar for 15 minutes unless otherwise stated. The solution was then irradiated with a blue LED (wavelength λ = 420 nm) or xenon lamp (225W Xe lamp equipped with 420 nm long pass filter (Edmund Industrial Optics) and CM-1 cold mirror, wavelength $420 \leq \lambda \leq 750$ nm) at 20 °C in a custom made aluminum box with cooling system. The amount of H_2 and CO_2 produced in the reaction was quantified by GC.

Product detection

The amount of H_2 and CO_2 produced at the headspace of the cell was quantified by a Shimadzu GC-2014 with a TCD detector equipped with a packed column with Molecular Sieve 5A (Ar carrier gas, 40 °C) and a packed column with Active Carbon 60/80 (He carrier gas, 80 °C), respectively. Calibration curves were obtained by sampling known amounts of H_2 and CO_2.

Properties of photosensitizers

The electrochemical and photochemical properties of photosensitizers $Ir(ppy)_3$, **Ir-2**, and **Ir-3** are summarized in Table 4.[31-33]

Table 4. The electrochemical and photochemical properties of photosensitizers.[31-33]

Photosensitizer	$Ir(ppy)_3$	**Ir-2**	**Ir-3**
$E_{1/2}(Ir^{III}/Ir^{II})$ (V *vs.* SCE)	−2.20	−1.51	−1.37
$E_{1/2}(Ir^{IV}/Ir^{III*})$ (V *vs.* SCE)	− 1.73	− 0.96	− 0.89
$E_{1/2}(Ir^{IV}/Ir^{III})$ (V *vs.* SCE)	0.78	1.21	1.69
E_{gap} (eV)	2.75	n/a	2.20
τ (ns)	1900	557	2300

Reference

1. K. Sordakis, C. Tang, L. K. Vogt, H. Junge, P. J. Dyson, M. Beller, G. Laurenczy, *Chem. Rev.*, **2018**, *118*, 372.
2. M. Iglesias and L. A. Oro, *Eur. J. Inorg. Chem.*, **2018**, *2018*, 2125.
3. C. Guan, Y. Pan, T. Zhang, M. J. Ajitha and K. -W. Huang, *Chem. Asian J.*, **2020**, *15*, 937.
4. R. S. Coffey, *Chem. Commun. (London)*, **1967**, 923b.
5. C. Fellay, P. J. Dyson and G. Laurenczy, *Angew. Chem. Int. Ed.*, **2008**, *47*, 3966.
6. S. Fukuzumi, T. Kobayashi and T. Suenobu, *J. Am. Chem. Soc.*, **2010**, *132*, 1496.
7. A. Boddien, D. Mellmann, F. Gärtner, R. Jackstell, H. Junge, P.J. Dyson, G. Laurenczy, R. Ludwig and M. Beller, *Science*, **2011**, *333*, 1733.
8. M. A. Esteruelas, C. García-Yebra, J. Martín and E. Oñate, *ACS Catal.*, **2018**, *8*, 11314.
9. W. Zhou, Z. Wei, A. Spannenberg, H. Jiao, K. Junge, H. Junge and M. Beller, *Chem. Eur. J.*, **2019**, *25*, 8459.
10. N. Lentz, A. Aloisi, P. Thuéry, E. Nicolas, and T. Cantat, *Organometallics*, **2021**, *40*, 565.
11. M. Onishi, *J. Mol. Catal.*, **1993**, *80*, 145.
12. B. Loges, A. Boddien, H. Junge, J. R. Noyes, W. Baumann and M. Beller, *Chem. Commun.*, **2009**, 4185.
13. A. Boddien, F. Gärtner, R. Jackstell, H. Junge, A. Spannenberg, W. Baumann, R. Ludwig and M. Beller, *Angew. Chem. Int. Ed.*, **2010**, *49*, 8993.
14. A. Boddien, B. Loges, F. Gärtner, C. Torborg, K. Fumino, H. Junge, R. Ludwig and M. Beller, *J. Am. Chem. Soc.*, **2010**, *132*, 8924.
15. S. M. Barrett, S. A. Slattery and A. J. M. Miller, *ACS Catal.*, **2015**, *5*, 6320.
16. C. -H. Chang, M. -H. Chen, W. -S. Du, J. Gliniak, J. -H. Lin, H. -H. Wu, H. -F. Chan, J. -S. K. Yu and T. -K. Wu, *Chem. Eur. J.*, **2015**, *21*, 6617.
17. Y. Sofue, K. Nomura and A. Inagaki, *Chem. Commun.*, **2020**, *56*, 4519.
18. D. Hong, Y. Shimoyama, Y. Ohgomori, R. Kanega, H. Kotani, T. Ishizuka, Y. Kon, Y. Himeda and T. Kojima, *Inorg. Chem.*, **2020**, *59*, 11976.
19. A. Boddien, F. Gärtner, C. Federsel, P. Sponholz, D. Mellmann, R. Jackstell, H. Junge and M. Beller, *Angew. Chem. Int. Ed.*, **2011**, *50*, 6411.
20. E. A. Bielinski, P. O. Lagaditis, Y. Zhang, B. Q. Mercado, C. Würtele, W. H. Bernskoetter, N. Hazari and S. Schneider, *J. Am. Chem. Soc.*, **2014**, *136*, 10234.
21. Y. Zhang, A. D. MacIntosh, J. L. Wong, E. A. Bielinski, P. G. Williard, B. Q.

Mercado, N. Hazari and W. H. Bernskoetter, *Chem. Sci.*, **2015**, *6*, 4291.
22. S. Enthaler, A. Brück, A. Kammer, H. Junge, E. Irran and S. Gülak, *ChemCatChem*, **2015**, *7*, 65.
23. J. B. Geri, J. L. Ciatti and N. K. Szymczak, *Chem. Commun.*, **2018**, *54*, 7790.
24. R. Tanaka, M. Yamashita and K. Nozaki, *J. Am. Chem. Soc.*, **2009**, *131*, 14168.
25. C. A. Huff and M. S. Sanford, *ACS Catal.*, **2013**, *3*, 2412.
26. Y. Yamazaki, H. Takeda and O. Ishitani, *J. Photochem. Photobiol. C.*, **2015**, *25*, 106.
27. H. Takeda, C. Cometto, O. Ishitani and M. Robert, *ACS Catal.*, **2017**, *7*, 70.
28. H. Takeda, H. Koizumi, K. Okamoto and O. Ishitani, *Chem. Commun.*, **2014**, *50*, 1491.
29. S. E. Lee, A. Nasirian, Y. E. Kim, P. T. Fard, Y. Kim, B. Jeong, S. -J. Kim, J. -O. Baeg and J. Kim, *J. Am. Chem. Soc.*, **2020**, *142*, 19142.
30. A. Zavras, M. Krstić, P. Dugourd, V. Bonačić-Koutecký and R. A. J. O'Hair, *ChemCatChem*, **2017**, *9*, 1298.
31. K. Teegardin, J. I. Day, J. Chan and J. Weaver, *Org. Process Res. Dev.*, **2016**, *20*, 1156.
32. M. S. Lowry, J. I. Goldsmith, J. D. Slinker, R. Rohl, R. A. Pascal, G. G. Malliaras and S. Bernhard, *Chem. Mater.*, **2005**, *17*, 5712.
33. A. Singh, K. Teegardin, M. Kelly, K. S. Prasad, S. Krishnan and J. D. Weaver, *J. Organomet. Chem.*, **2015**, *776*, 51.

Chapter 3

Metal ion substitution in a pentanuclear scaffold provides an efficient catalyst for a CO_2/HCOOH cycle

Introduction

The growing demand for energy and the ongoing depletion of fossil fuels have prompted much effort to develop renewable and environmentally friendly energy sources. Hydrogen gas is known as an energy carrier and a clean alternative to conventional fossil fuels. However, the gaseous nature of hydrogen makes storage and transport difficult. Given this background, the liquid organic hydrogen carrier HCOOH has been recognised as a promising candidate because of its high H_2 content and low toxicity.[1] However, for the utilization of HCOOH as a hydrogen carrier, it is crucial to develop efficient catalysts for the production of HCOOH and its conversion into hydrogen.

Conventionally, the production of HCOOH[2-8] and its conversion into hydrogen[9-19] have been achieved via a reversible hydrogenation/dehydrogenation cycle between CO_2 and HCOOH.[15-19] However, this cycling process requires the utilization of gaseous hydrogen as well as high pressure and temperature conditions for the production of HCOOH. In Chapter 2, I reported a novel cycle for the production of HCOOH and its conversion into hydrogen, which involves the two-electron reduction of CO_2 and the dehydrogenation of HCOOH. This cycle enables both the formation of HCOOH from CO_2 and protons and the dehydrogenation of HCOOH under visible-light irradiation at ambient pressure and temperature. Notably, the maximum TOF of the system for the photochemical dehydrogenation reaction was the highest (229 h^{-1}) among the relevant catalytic systems.[20-23] These results indicate that our newly proposed cycle can be an attractive alternative for achieving efficient utilization of HCOOH. However, further improvement in the activity and selectivity is crucial for future practical applications.

In this chapter, I constructed an efficient photocatalytic cycle for the CO_2 reduction/dehydrogenation of HCOOH based on the pentanuclear copper complex $[Cu_5OH(bpp)_6]^{3+}$ (**Cu5**). **Cu5** can catalyze the dehydrogenation of HCOOH with higher activity than **Co5**. Under the optimal conditions, the TOF of **Cu5** for the dehydrogenation of HCOOH reached 323 h^{-1}, which was significantly higher than that of my previous best catalyst **Co5** (229 h^{-1}).

There are two important keys to our success: the employment of (1) a pentanuclear scaffold and (2) appropriate metal ions. The pentanuclear scaffold ($[M_5OH(bpp)_6]^{n+}$) can serve as a catalyst for small molecule conversions because of its excellent electron

transfer ability owing to its five metal ions and substrate-activation ability owing to the presence of coordinatively unsaturated sites.[24-27] Indeed, **Co5** can serve as a dual-catalyst for the photoinduced two-electron reduction of CO_2 and dehydrogenation of HCOOH. The previous study also revealed that the one-electron-reduced species of the scaffold and the multinuclear metal center play important roles in the catalysis. Therefore, the facile formation of one-electron-reduced species and the presence of a highly active multinuclear metal center are crucial. In this regard, the use of copper ions can be an excellent strategy because (i) copper ions can be easily reduced, and (ii) copper-based multinuclear centers can facilitate decarboxylation to form hydride species.[28]

Results and discussions

Synthesis and characterization

A pentanuclear copper complex (**Cu5**) was synthesised according to previously reported procedures[29]: a methanol solution of Hbpp ligand and copper acetate monohydrate (1.3 eq.) was refluxed for 30 min. After the reaction, a few drops of saturated aqueous solution of $NaClO_4$ were added. The obtained precipitate was dissolved in a mixture of acetonitrile and water, and the slow evaporation of acetonitrile afforded the target compound as green crystals in 30% yield. The compound was characterised using ESI-TOF MS and elemental analysis. ESI-TOF-MS: m/z: 553.4 $[Cu_5OH(bpp)_6]^{3+}$. Elemental analysis calcd. (%) for $C_{78}H_{59}Cl_3Cu_5N_{24}O_{15}$: C,46.92; H, 2.98; N, 16.84. Found: C, 47.05; H, 3.04; N, 16.55. The structure of the complex was determined using single-crystal X-ray structural analysis (Figure 1 and Table 1), confirming the formation of a pentanuclear structure. In IR spectrum of **Cu5**, the peak at 3500 cm^{-1} assigned with O-H stretching mode indicate μ_3-OH bridging moiety (Figure 2).

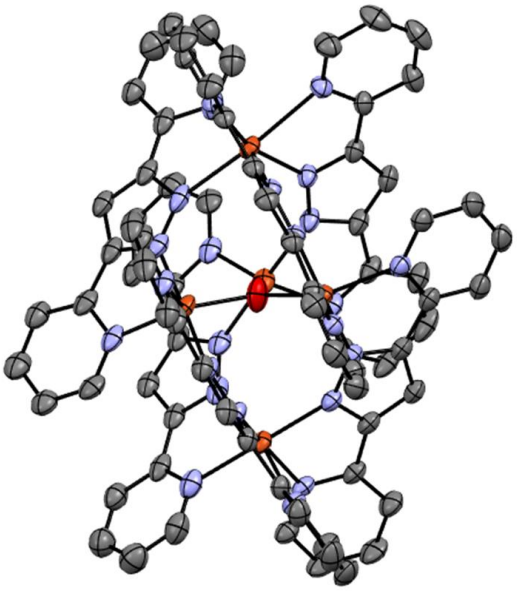

Figure 1. ORTEP drawing of the cationic moiety of **Cu5**$(ClO_4)_3$. The atoms are represented by the following colors: Cu, orange; O, red; N, purple; C, gray. Hydrogen atoms, counter anions and crystal solvent molecules are omitted for clarity.

Table 1. Summary of crystallographic data for **Cu5**.

	$[Cu_5OH(bpp)_6](ClO_4)_3$
formula	$C_{78}H_{55}Cl_3Cu_5N_{24}O_{13}$
crystal system	monoclinic
space group	*C2/c*
a /Å	16.3591(3)
b /Å	25.4257(5)
c /Å	22.6532(4)
β /°	98.634(2)
V /Å^3	9315.6(3)
Z	4
R_1	0.0460
wR_2	0.1202
GooF	1.053

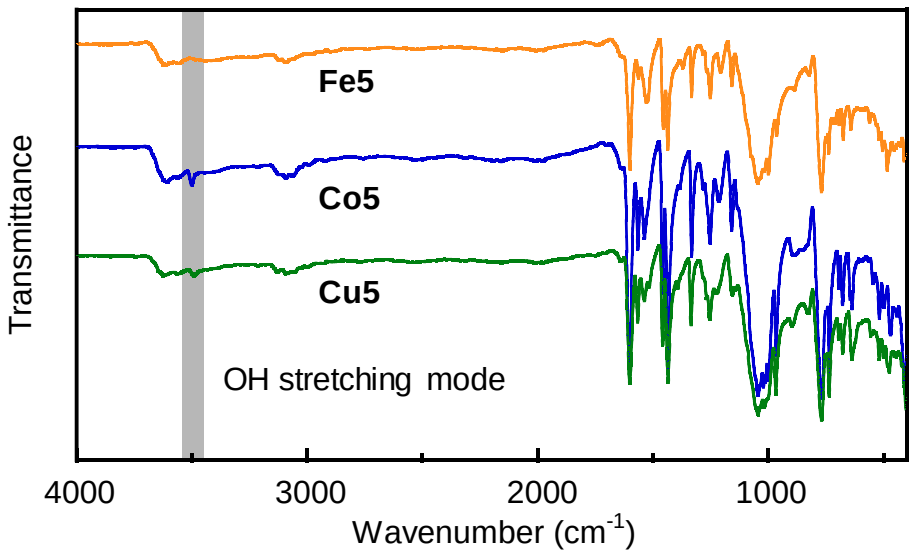

Figure 2. IR spectra of **Fe5**$(BF_4)_3$ (orange line), **Co5**$(BF_4)_3$ (blue line), and **Cu5**$(BF_4)_3$ (green line).

Electrochemical measurement

Subsequently, cyclic voltammetry was performed to investigate the redox properties of **Cu5** (Figure 3). In the CV of **Cu5** under Ar atmosphere (Figure 3, green line), the complex displayed two reduction waves at $E_{1/2}$ = −0.78 and −0.94 V (*vs.* Fc/Fc^+). These redox waves can be attributed to the one-electron reduction of the copper ions. The redox potentials of **Cu5** and the relevant pentanuclear complex **Co5**, are summarized in Table 2. As I showed in Chapter 1, **Co5** exhibits three reversible reduction waves at $E_{1/2}$ = −1.72, −1.96, and −2.19 V (*vs.* Fc/Fc^+; Figure 3, blue line), which are attributable to the reduction of the cobalt center at the triangular core. The first reduction wave of **Cu5** was located at a more positive potential than that of **Co5**. As expected (*vide supra*), **Cu5** can generate one-electron-reduced species, which are expected to function as key intermediates for the dehydrogenation of HCOOH, more easily than **Co5**.

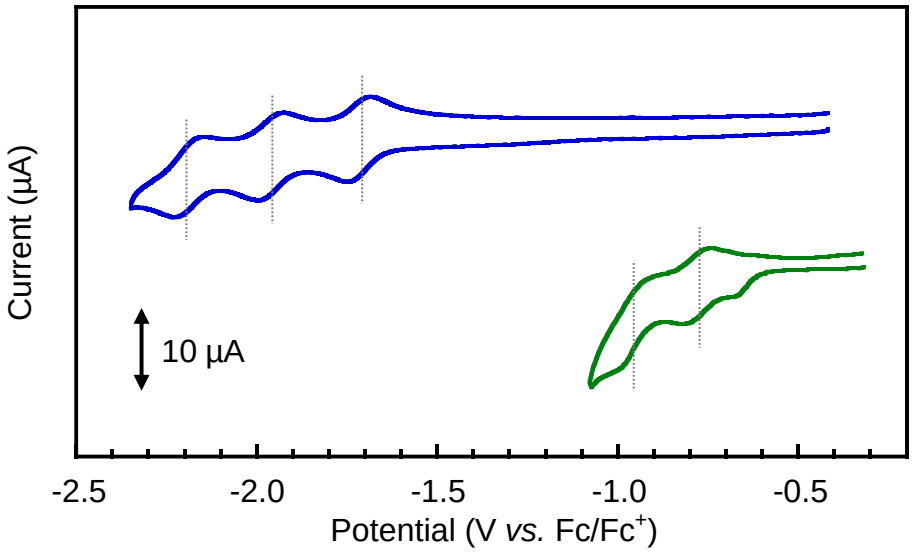

Figure 3. Cyclic voltammograms of 0.2 mM solutions of **Co5** (blue line) and **Cu5** (green line) under Ar in MeCN containing 0.1 M TBAP. The CVs were measured using a GC electrode at a scan rate of 100 mVs^{-1}.

Table 2. Electrochemical properties of penta-nuclear metal complexes (**Co5** and **Cu5**).

complex	$E_{1/2}$ (V *vs.* Fc/Fc^+)				
	$M^{II/I}$			$M^{III/II}$	
Co5	−2.19	−1.96	−1.72	−0.30	−0.11
Cu5	-	−0.94	−0.78	-	-

Photochemical formic acid dehydrogenation

I then investigated the photocatalytic activity of **Cu5** for the dehydrogenation of HCOOH. The reaction was performed in 2 mL of DMA solution containing **Cu5** (30 μM) as the catalyst, $Ir(ppy)_3$ (150 μM) as the photosensitizer, BIH (25 mM) as the sacrificial electron donor, and HCOOH (500 *eq. vs.* **Cu5**) as the substrate in an Ar atmosphere under visible-light irradiation (blue LED, wavelength λ = 420 nm) at 20 °C. As shown in Figure 4, evolution of hydrogen gas was observed after 3 h of photoirradiation (TON = 142). As a control experiment, the reaction was performed using TFA instead of HCOOH as the substrate. In this case, only a trace amount of hydrogen was detected, confirming that hydrogen was produced not by proton reduction but by the dehydrogenation of HCOOH. The hydrogen production activity of **Cu5** *via* dehydrogenation of HCOOH was higher than that of **Co5** (TON = 106) under identical conditions. These results demonstrate that **Cu5** can catalyze the photoinduced dehydrogenation of HCOOH with better performance than **Co5**.

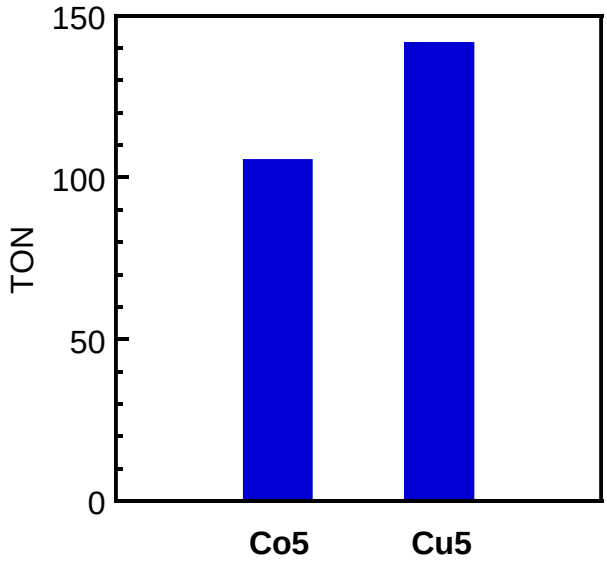

Figure 4. Photochemical HCOOH dehydrogenation activities in the presence of **Co5** (left bar) or **Cu5** (right bar). Reactions were performed in Ar saturated DMA solution containing 30 μM catalyst, 150 μM $Ir(ppy)_3$ and 25 mM BIH under irradiation of visible light (blue LED, wavelength λ = 420 nm).

To gain further insight into the **Cu5**-mediated dehydrogenation of HCOOH, the photosensitizer was investigated. In this experiment, $[Ir(dF(CF_3)ppy)_2(dtbbpy)](PF_6)$ (**Ir-3**) was used as the photosensitizer. The reaction between **Cu5** and **Ir-3** resulted in hydrogen production (Figure 5). By contrast, the reaction using **Co5** as the catalyst and **Ir-2** as the photosensitiser did not produce hydrogen. These results can be interpreted considering the redox potentials of **Ir-3**, **Cu5** and **Co5**. The redox potential of **Ir-3** locates at $E_{1/2}(Ir^{III}/Ir^{II}) = -1.74$ V (*vs.* Fc/Fc^+), and the first reduction potentials of **Cu5** and **Co5** locate at −0.78 and −1.72 V, respectively. Therefore, although **Ir-3** can reduce **Cu5**, it is difficult to reduce **Co5**. As demonstrated in Chapter 2, the formation of a one-electron-reduced species with Co^I at the triangular core of **Co5** is essential for the reaction. The aforementioned results indicate that, similar to **Co5**, the one-electron-reduced species of **Cu5** were involved in the reaction. CV measurements in the presence of **Cu5** and HCOOH also supported this hypothesis (Figure 6). The current at the first reduction peak of **Cu5** is slightly higher than that in the absence of HCOOH, indicating specific interactions between the one-electron-reduced species of **Cu5** and HCOOH. These results indicate that **Cu5** catalyzes the dehydrogenation of HCOOH *via* the formation of one-electron-reduced species, while the decrease in the first reduction potential affords a catalytic system that operates under milder conditions (i.e., with the use of a photosensitizer with lower reducing ability) than that of **Co5**.

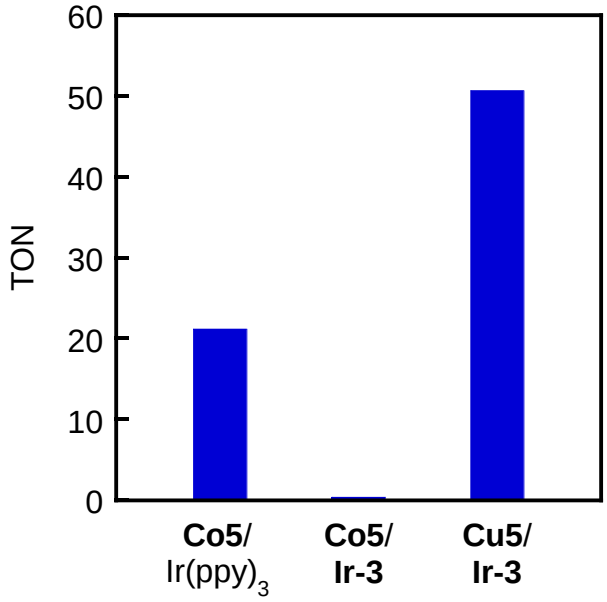

Figure 5. Photochemical formic acid dehydrogenation activities by a combinations of catalysts (**Co5** or **Cu5**) and photosensitisers ($Ir(ppy)_3$ or **Ir-2**). Reactions were performed in Ar saturated DMA solution containing 30 μM catalyst, 150 μM $Ir(ppy)_3$ and 100 mM BIH under irradiation of visible light (blue LED, wavelength λ = 420 nm).

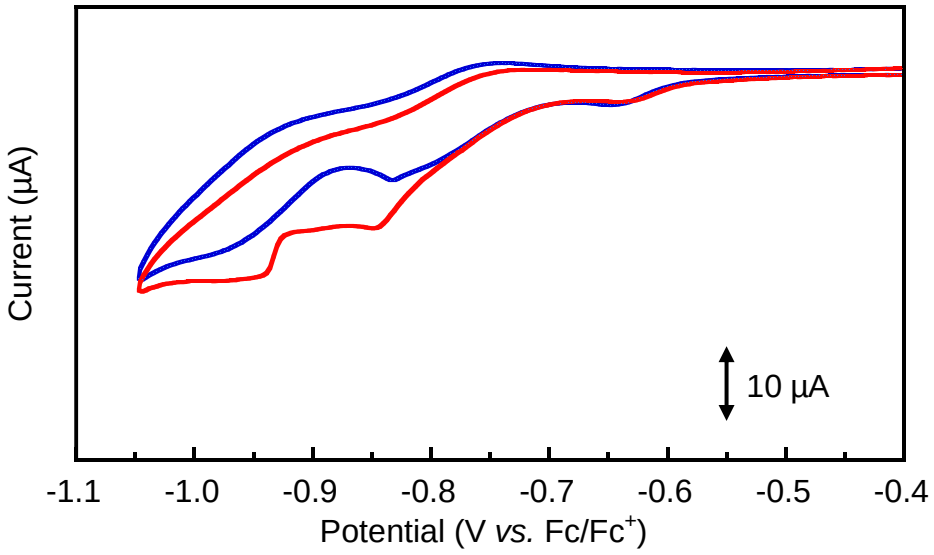

Figure 6. Cyclic voltammograms of 0.2 mM solution of **Cu5** in the presence (red line) and in the absence (blue line) of 0.5 *eq.* formic acid (0.1 mM) in MeCN containing 0.1 M TBAP. The CVs were measured using a GC electrode at a scan rate of 10 mVs^{-1}.

Photochemical CO_2 reduction

The catalytic activity of **Cu5** for CO_2 reduction was investigated. Photochemical reactions were conducted under CO_2 in a DMA/trifluoroethanol (17:3, v/v) solution containing **Cu5** (30 μM) as the catalyst, $Ir(ppy)_3$ (150 μM) as the photosensitizer, and BIH (100 mM) as the sacrificial electron donor under visible-light irradiation (blue LED, λ = 420 nm). The photoinduced CO_2 reduction proceeded successfully, and the formation of CO, HCOOH, and hydrogen, which appears to be a product of HCOOH dehydrogenation, was confirmed (Figure 7). Similar to the catalytic system of **Co5**, this is a rare example of a hydrogen storage/release cycle based on the photochemical reduction of CO_2 and the dehydrogenation of HCOOH. Although the TON for CO production of **Cu5** (TON_{CO} = 3.1) is lower than that of **Co5** (TON_{CO} = 3.4), those for HCOOH and hydrogen production were higher in **Cu5** (TON_{HCOOH} = 4.2 (**Cu5**) and 1.8 (**Co5**), and TON_{H2} = 6.5 (**Cu5**) and 2.8 (**Co5**)). Given that the evolved hydrogen originated from HCOOH dehydrogenation, the total TON of **Cu5** and **Co5** for HCOOH production was calculated to be 10.7 and 4.6, respectively. Therefore, the selectivity for HCOOH production was significantly enhanced in the **Cu5**-based catalytic system (78% for **Cu5** and 57% for **Co5**). These results clearly demonstrate that the incorporation of copper ions into the pentanuclear scaffold greatly enhanced the activity and selectivity for HCOOH formation *via* CO_2 reduction.

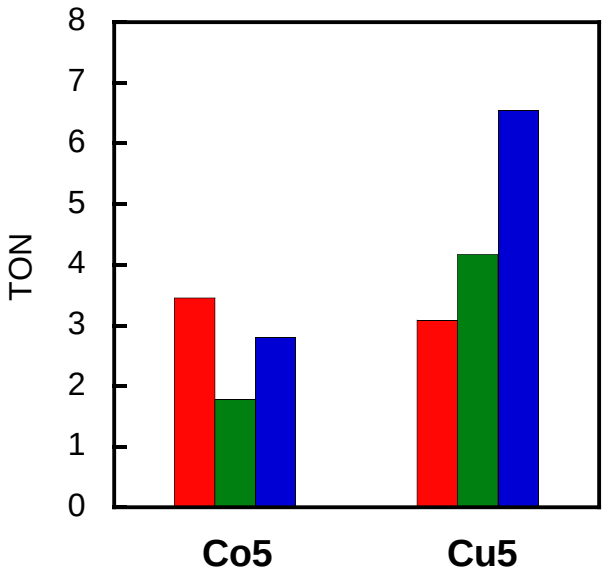

Figure 7. Photocatalytic production of CO (red), HCOOH (green) and H_2 (blue). Reactions were performed in CO_2 saturated DMA solution containing 30 μM catalyst, 150 μM $Ir(ppy)_3$ and 100 mM BIH and trifluoroethanol under irradiation of visible light (blue LED, wavelength λ = 420 nm).

Possible mechanism

A possible catalytic mechanism for photochemical dehydrogenation of HCOOH by **Cu5** is shown in Scheme 1. First, the copper ion of **Cu5** is reduced by a photosensitizer. On the basis of the catalytic activity of **Cu5** with **Ir-3** (Figure 5) and CV measurements of **Cu5** in the presence of HCOOH (Figure 6), it was found that active species could be formed more easily than in the case of **Co5**. This reduced species reacts with HCOOH to release hydrogen and CO_2. Our system is similar to that reported by Meyer *et al.*, who elucidated the formation of a hexacopper(I) dihydride cluster from the reduction-induced decarboxylation of a dicopper(II) formate complex.[28] Other copper complexes that work as catalysts for the dehydrogenation of HCOOH contain Cu^I as a reaction intermediate.[30-33] Based on these examples, Cu^I is assumed to promote the reaction with HCOOH. Moreover, it has been reported that the synergistic effect between distinct metal ions plays an important role in the dehydrogenation reaction.[31,34] Thus, the multinuclear metal structures of **Co5** and **Cu5** are effective for catalysis. In addition to participating in the HCOOH dehydrogenation reaction, **Cu5** also reacts with the CO_2 generated during the dehydrogenation reaction; the electron-reduced species of **Cu5** reduces CO_2 to HCOOH or CO (CO_2 reduction process). Therefore, the dual-catalysis mechanism explains both the dehydrogenation of HCOOH as well as the two-electron reduction of CO_2 mediated by **Cu5**.

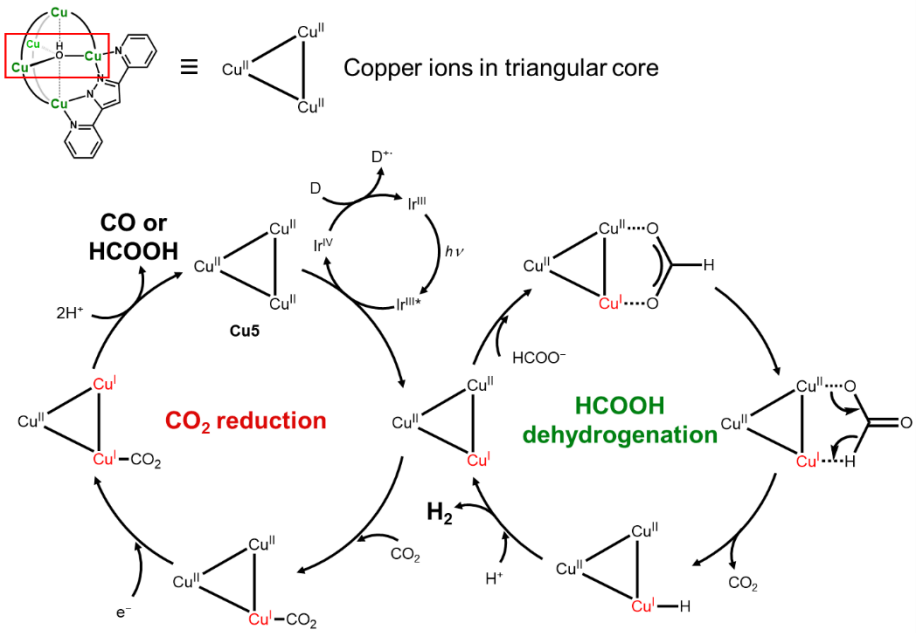

Scheme 1. Proposed mechanism of the dual catalysis process mediated by **Cu5**. Dehydrogenation of formic acid (right) and two-electron reduction of CO_2 (left).

Optimization

Finally, the reaction conditions for HCOOH dehydrogenation were optimized. Upon increasing the concentration of HCOOH to 25 mM (1000 eq. versus **Cu5**) and under photoirradiation with a Xe lamp ($420 < \lambda < 750$ nm), the maximum TON for the reaction increased to 323 after 1 h. In Chapter 2, I demonstrated that the TOF of **Co5** for the HCOOH dehydrogenation reaction (229 h^{-1}) was the highest observed to date for molecular catalysts that operate under photoirradiation at ambient temperatures. The current study demonstrates that the TOF (323 h^{-1}) of **Cu5** is higher than that of **Co5**, and is the highest among those reported for the relevant catalysts (Table 3).

Table 3. Comparison of catalytic activity of the pentanuclear catalysts for photochemical HCOOH dehydrogenation.

catalyst	Concentration	Temp. (°C)	TON (time)	TOF (h^{-1})[a]
Cu5	0.03 mM	r.t.	323 (1 h)	323
Co5	0.03 mM	r.t.	229 (1 h)	229

[a] The turnover frequency (TOF, h^{-1}) was calculated by dividing the turnover number (TON) with duration of photoirradiation.

Conclusion

I successfully demonstrated that metal ion substitution in a pentanuclear metal complex can afford a highly efficient photocatalytic cycle for CO_2 reduction/HCOOH dehydrogenation (CO_2/HCOOH cycle). I synthesized a pentanuclear copper complex (**Cu5**) and investigated its photocatalytic activity for HCOOH dehydrogenation. The reactions proceeded under photoirradiation in the presence of **Cu5**, a photosensitizer, and a sacrificial electron donor at ambient temperature and pressure. **Cu5** catalyzed both the HCOOH dehydrogenation reaction and CO_2 reduction with higher activity than previously synthesized **Co5**. This study offers a novel strategy for the efficient utilization of HCOOH as a hydrogen carrier.

Experimental Section

Materials

$Ir(ppy)_3$, formic acid, trifluoroacetic acid, and all the solvents except for *N,N*-dimethylacetamide (DMA) were purchased from FUJIFILM Wako Pure Chemical Corporation. Tetra-*n*-butylammonium perchlorate (TBAP), and DMA were purchased from Tokyo Chemical Industry Co., Ltd. $[Ir(dF(CF_3)ppy)_2(dtbbpy)](PF_6)$ was purchased from Aldrich. All the reagents were of highest quality available and were used as received except for TBAP. TBAP was recrystallized from absolute ethanol. H_2O was purified using a Millipore MilliQ purifier.

Synthesis of a pentanuclear cupper complex (Cu5)

A pentanuclear copper complex (**Cu5**) was prepared according to our previously reported procedures.[29] Aqueous solution of NaOH (1 M, 0.6 mL) was added to the methanol solution (5 mL) of 3,5-bis(2-pyridyl)pyrazole (Hbpp, 0.60 mmol, 133 mg). $Cu(CH_3COO)_2 \cdot H_2O$ (0.80 mmol, 160 mg) was then added to the reaction mixture and refluxed for 30 minutes. A few drops of saturated aqueous $NaClO_4$ solution was added to the reaction mixture, and a small portion of water was added to the solution. The solution was kept in a refrigerator for 30 minutes to generate a green precipitate. The precipitate was collected by filtration, washed with water and dried under vacuum. The obtained precipitate was dissolved in acetonitrile/water (4:3 v/v) and slow evaporation of acetonitrile at ambient temperature gave green crystals of $[Cu^{II}_5OH(bpp)_6](ClO_4)_3 \cdot 2H_2O$. The crystals were collected by filtration and dried under vacuum. Yield 59.9 mg (30%). Elemental analysis calcd. (%) for $C_{78}H_{59}Cl_3Cu_5N_{24}O_{15}$: C, 46.92; H, 2.98; N, 16.84. Found C, 46.86; H, 3.13; N, 16.69.

X-ray crystallography

Crystals were obtained by slow vapor diffusion of *tert*-butyl methyl ether into acetonitrile solution of **Cu5**. The crystal of **Cu5** was mounted in a loop. Data collection for **Cu5** was performed at 293 K on a ROD, Synergy Custom system (Rigaku Oxford Diffraction) equipped with confocal monochromated Mo-Ka radiation, and data was processed using CrysAlisPro 1.171.39.43c (Rigaku) system software. The structure was solved by direct methods using SHELXT program[35] through the Olex2 interface.[36] All-non-hydrogen atoms were refined anisotropically by a least-squares method, and hydrogen atoms were fixed at calculated positions and refined using a riding model. SHELXL-2014/7[37] was used for structural refinement. Full-matrix least-squares refinements on F^2 based on unique reflections with unweighted and weighted agreement factor of $R = \Sigma||F_o| - |F_c||/\Sigma|F_o|$ ($I > 2.00\ \sigma(I)$) and $wR = [\Sigma w(F_o^2 - F_c^2)^2/\Sigma w(F_o^2)^2]^{1/2}$ were performed. The diffused electron densities resulting from residual solvent molecules were removed from the data set using the SQUEEZE routine and refined further using the data generated. Crystallographic data have been deposited with Cambridge Crystallographic Data Centre: CCDC deposition number; 2219980 for **Cu5**$(ClO_4)_3$. Copies of the data can be obtained free of charge vis www.ccdc.cam.ac.uk/data_request/cif.

Electrochemical studies

Cyclic voltammetry was performed with a Bio-Logic-Science Instruments potentiostat interfaced to a computer with SP-50 software, at room temperature under Ar using one-compartment cell with a standard three-electrode configuration, which consisted of a glassy carbon disk (diameter 3 mm, from BAS Inc.), a Ag/Ag^+ couple, and a platinum wire as the working, reference, and auxiliary electrodes, respectively. The working electrode was treated between scans by means of polishing with 0.05 μm alumina paste (from BAS Inc.) and washing with purified H_2O. Ferrocene was used as an internal standard, and all potentials reported within this work are referenced to the ferrocenium/ferrocene couple at 0 V.

Photochemical HCOOH dehydrogenation reaction

For a typical run, a mixed solution of DMA (2.0 mL) containing 30 μM catalyst, 150 μM $Ir(ppy)_3$ and 25 mM BIH, and HCOOH (13 mM, 500 *eq. vs.* **Cu5**) was purged with Ar for 15 minutes unless otherwise stated. The solution was then irradiated with a blue LED (wavelength λ = 420 nm) or xenon lamp (225W Xe lamp equipped with 420 nm long pass filter (Edmund Industrial Optics) and CM-1 cold mirror, wavelength $420 \leq \lambda \leq 750$ nm) at 20 °C in a custom made aluminum box with cooling system. The amount of H_2 and CO_2 produced in the reaction was quantified by GC.

Photochemical CO_2 reduction reaction

For a typical run, a mixed solution of DMA/TFE (17:3, v/v) (2.0 mL) containing 30 μM **Cu5**, 150 μM $Ir(ppy)_3$ and 0.10 M BIH was purged with CO_2 for 15 minutes unless otherwise stated. The solution was then irradiated with a blue LED (wavelength λ = 420 nm) at 20 °C in a custom made aluminium box with cooling system. The amount of CO, H_2 and HCOOH produced in the reaction was quantified by GC and LC.

Product detection

The amount of CO and H_2 produced at the headspace of the cell was quantified by a Shimadzu GC-2014 with a TCD detector equipped with a packed column with Molecular Sieve 13X-S 60/80 (He carrier gas, 40 °C) and Molecular Sieve 5A (Ar carrier gas, 40 °C), respectively. Additionally, the liquid product was quantified by using a Shimadzu LC-20AD with SPD-20A and RID-10A detectors equipped with a Shim-pack SCR 102H column. Calibration curves were obtained by sampling known amounts of CO, H_2, and HCOOH.

Reference

1. K. Sordakis, C. Tang, L. K. Vogt, H. Junge, P. J. Dyson, M. Beller and G. Laurenczy, *Chem. Rev.*, **2018**, *118*, 372.
2. R. Tanaka, M. Yamashita and K. Nozaki, *J. Am. Chem. Soc.*, **2009**, *131*, 14168.
3. C. A. Huff and M. S. Sanford, *ACS Catal.*, **2013**, *3*, 2412.
4. Y. Zhang, A. D. MacIntosh, J. L. Wong, E. A. Bielinski, P. G. Williard, B. Q. Mercado, N. Hazari and W. H. Bernskoetter, *Chem. Sci.*, **2015**, *6*, 4291.
5. Y. Yamazaki, H. Takeda and O. Ishitani, *J. Photochem. Photobiol. C*., **2015**, *25*, 106.
6. H. Takeda, C. Cometto, O. Ishitani and M. Robert, *ACS Catal.*, **2017**, *7*, 70.
7. H. Takeda, H. Koizumi, K. Okamoto and O. Ishitani, *Chem. Commun.*, **2014**, *50*, 1491.
8. S. E. Lee, A. Nasirian, Y. E. Kim, P. T. Fard, Y. Kim, B. Jeong, S. -J. Kim, J. -O. Baeg and J. Kim, *J. Am. Chem. Soc.*, **2020**, *142*, 19142.
9. R. S. Coffey, *Chem. Commun. (London)*, **1967**, 923b.
10. A. Boddien, D. Mellmann, F. Gärtner, R. Jackstell, H. Junge, P. J. Dyson, G. Laurenczy, R. Ludwig and M. Beller, *Science*, **2011**, *333*, 1733.
11. M. C. Neary and G. Parkin, *Dalton Trans.*, **2016**, *45*, 14645.
12. M. A. Esteruelas, C. García-Yebra, J. Martín and E. Oñate, *ACS Catal.*, **2018**, *8*, 11314.
13. A. Léval, A. Agapova, C. Steinlechner, E. Alberico, H. Junge and M. Beller. *Green Chem.*, **2020**, *22*, 913.
14. N. Lentz, A. Aloisi, P. Thuéry, E. Nicolas, and T. Cantat, *Organometallics*, **2021**, *40*, 565.
15. A. Boddien, F. Gärtner, C. Federsel, P. Sponholz, D. Mellmann, R. Jackstell, H. Junge and M. Beller, *Angew. Chem. Int. Ed.*, **2011**, *50*, 6411.
16. F. Bertini, I. Mellone, A. Ienco, M. Peruzzini and L. Gonsalvi, *ACS Catal.*, **2015**, *5*, 1254.
17. S. Enthaler, A. Brück, A. Kammer, H. Junge, E. Irran and S. Gülak, *ChemCatChem*, **2015**, *7*, 65.
18. J. Fidalgo, M. Ruiz-Castañeda, G. García-Herbosa, A. Carbayo, F. A. Jalón, A. M. Rodríguez, B. R. Manzano and G. Espino, *Inorg. Chem.*, **2018**, *57*, 14186.
19. J. B. Geri, J. L. Joanna and N. K. Szymczak, *Chem. Commun.*, **2018**, *54*, 7790.
20. M. Onishi, *J. Mol. Catal.*, **1993**, *80*, 145.
21. A. Boddien, B. Loges, F. Gärtner, C. Torborg, K. Fumino, H. Junge, R. Ludwig and

M. Beller, *J. Am. Chem. Soc.*, **2010**, *132*, 8924.
22. S. M. Barrett, S. A. Slattery, and A. J. M. Miller, *ACS Catal.*, **2015**, *5*, 6320.
23. Y. Sofue, K. Nomura and A. Inagaki, *Chem. Commun.*, **2020**, *56*, 4519.
24. M. Okamura, M. Kondo, R. Kuga, Y. Kurashige, T. Yanai, S. Hayami, V. K. K. Praneeth, M. Yoshida, K. Yoneda, S. Kawata, and S. Masaoka, *Nature*, **2016**, *530*, 465.
25. V. K. K. Praneeth, M. Kondo, M. Okamura, T. Akai, H. Izu and S. Masaoka, *Chem. Sci.*, **2019**, *10*, 4628.
26. M. Kondo, S. Masaoka, *Acc. Chem. Res*., **2020**, *53*, 2140.
27. H. Izu, M. Kondo, M. Okamura, M. Tomoda, S. K. Lee, T. Akai, V. K. K. Praneeth, M. Kanaike, S. Kawata and S. Masaoka, *ChemRxiv Preprint*, DOI: 10.33774/chemrxiv-2021-n3jtl.
28. J. Lucken, T. Auth, S. I. Mozzi and F. Meyer, *Inorg. Chem.*, **2020**, *59*, 14347.
29. R. Ishikawa, M. Nakano, A. Fuyuhiro, T. Takeuchi, S. Kimura, T. Kashiwagi, M. Hagiwara, K. Kindo, S. Kaizaki and S. Kawata, *Chem. Eur. J.*, **2010**, *16*, 11139.
30. N. Scotti, R. Psaro, N. Ravasio and F. Zaccheria, *RSC Adv.*, **2014**, *4*, 61514.
31. A. Zavras, M. Krstic, P. Dugourd, V. Bonačić-Koutecký and R. A. J. O'Hair, *ChemCatChem*, **2017**, *9*, 1298.
32. T. Nakajima, Y. Kamiryo, M. Kishimoto, K. Imai, K. Nakamae, Y. Ura and T. Tanase, *J. Am. Chem. Soc.*, **2019**, *141*, 8732.
33. A. N. Desnoyer, A. Nicolay, M. S. Ziegler, N. A. Torquato and T. D. Tilley, *Angew. Chem. Int. Ed.*, **2020**, *59*, 12769.
34. D. Hong, Y. Shimoyama, Y. Ohgomori, R. Kanega, H. Kotani, T. Ishizuka, Y. Kon, Y. Himeda and T. Kojima, *Inorg. Chem.*, **2020**, *59*, 11976.
35. G. M. Sheldrick, *Acta Cryst*., **2015**, *A71*, 3.
36. O. V. Dolomanov, L. J. Bourhis, R. J. Gildea, J. A. K. Howard and H. Puschmann, *J. Appl. Crystallogr.*, **2009**, *42*, 339.
37. G. M Sheldrick., *Acta Cryst.*, **2015**, *C71*, 3.

Concluding Remarks

The research reported in this thesis has developed pentanuclear metal complex-based catalysts for a novel CO_2/HCOOH cycle constructed with the two-electron reduction of CO_2 and the dehydrogenation of HCOOH.

In chapter 1, I substituted metal ions of **Fe5** with cobalt ions and synthesized a novel pentanuclear cobalt complex (**Co5**). Electrochemical measurements revealed that **Co5** exhibits multielectron reduction ability, making it completely distinct from **Fe5**, which shows multielectron oxidation ability. Moreover, the cyclic voltammetry of **Co5** under CO_2 indicates the catalytic activity of the complex for CO_2 reduction. I demonstrated that **Co5** reduces CO_2 to CO and HCOOH under electrochemical and photochemical conditions.

In chapter 2, I investigated the catalytic activity of **Co5** for photochemical HCOOH dehydrogenation reaction. The dehydrogenation reactions were performed under photoirradiation in the presence of **Co5**, a suitable photosensitizer, and sacrificial electron donor at ambient temperature and resulted in the generation of H_2 and CO_2, and its activity is higher than those of similar previously reported molecular catalysts. Given that **Co5** also catalyzes the photochemical two-electron reduction of CO_2 into HCOOH, this study is the first example of a CO_2/HCOOH cycle based on the photochemical reduction of CO_2 and dehydrogenation of HCOOH.

In chapter 3, I developed an efficient catalyst for a photocatalytic HCOOH/CO_2 cycle by metal ion substitution in a pentanuclear scaffold. I synthesized a pentanuclear copper complex (**Cu5**) and investigated its photocatalytic activity for HCOOH dehydrogenation and CO_2 reduction. I demonstrated that **Cu5** catalyzes both the HCOOH dehydrogenation reaction and CO_2 reduction with higher activity than **Co5**.

Collectively, the results in this thesis have shown that pentanuclear metal complex based catalysts construct an unconventional CO_2/HCOOH cycle composed of two-electron CO_2 reduction and HCOOH dehydrogenation. The use of multinuclear metal complexes with multielectron transfer and bond formation/cleavage ability is one of the strategies to develop catalysts for CO_2 utilization. Metal ion substitution in a multinuclear metal scaffold is also a significant strategy to develop catalysts. I believe that these results should facilitate the development of a variety of multinuclear-metal-based catalysts for sustainable CO_2 utilization.

Acknowledgments

The presented thesis is the summary of the author's studies at the Department of Structural Molecular Science, School of Physical Science, the Graduate University for Advanced Studies (SOKENDAI) (from April 2018 to May 2019) and at the Division of Applied Chemistry, Graduate School of Engineering, Osaka University (from June 2019 to January 2023) under the direction of Professor Shigeyuki Masaoka.

First of all, I would like to express my deepest gratitude to Professor Shigeyuki Masaoka for his significant guidance, and impassioned encouragement. I could learn much from him not only chemistry but also the passion toward science. I am deeply grateful to Associate Professor Mio Kondo for her helpful suggestion and heartfelt encouragement. I would like to thank Assistant Professor Yutaka Saga for his helpful advice.

I express sincere appreciation to alumni of Masaoka Group in Institute for Molecular Science, Dr. Masaya Okamura, Dr. Vijayendran K. K. Praneeth, Dr. Pondchanok Chinapang, Dr. Arisa Fukatsu, Dr. Takafumi Enomoto, Dr. Lee Sze Koon, Dr. Hitoshi Izu, Dr. Hikaru Iwami, Ms. Mami Kachi, Mr. Masahiro Tasaki, Ms. Mei Ishihara, Mr. Soshi Kato, Ms. Mayu Fujisawa, and Ms. Miho Matsuda for many advice about research, valuable discussion, heartfelt encouragement and friendship during my time in the lab.

I also express my appreciation to our current and alumni members of Masaoka Group in Osaka University, Dr. Kento Kosugi, Dr. Zi Lang Goo, Ms. Misa Tomoda, Ms. Chiharu Akatsuka, Mr. Hayato Tatewaki, Mr. Ryo Tomiyasu, Mr. Yusuke Nakayama, Mr. Hirotaka Hamaguchi, and Mr. Shinki Fujisawa, Ms. Zhi Yang, Ms. Kanako Okuda, Ms. Hina Kashima, Mr. Toshimichi Kobayashi, Mr. Nozomi Yamaguchi, Mr. Taito Watanabe, Mr. Shangxing Li Mr. Maho Imai, Mr. Masaki Kitada, Ms. Yuka Kiyokawa, Mr. Takumi Matsuzaki, Mr. Yuma Morii, Ms. Yumi Iwamura, Mr. Xianjun Li, Mr. Marc Alec Dominic Yau, Ms. Nayu Kageyama, Ms. Senri Katsuhira, Mr. Masaya Sakamoto, Ms. Minami Fukuhara, Mr. Chuanyuan Liu for advices about research, precious discussion, heartfelt encouragement and friendship during my time in the lab. I appreciate the assistance from secretaries, Ms. Kyoko Kawashima and Ms. Kiyomi Lee for administration supports. My special thanks are due to Ms. Yumi Iwamura who advance the research with me.

I would like to acknowledge Associate Professor Chihiro Kachi in Toho university for

precise guidance and heartfelt encouragement. I would like to thank members of Kachi group for their discussions and friendships.

I would like to thank for the financial support from JST SPRING.

Finally, I would like to express my greatest appreciation to my family, Yoshio Akai, Kayoko Akai, Naoki Akai for their continuous, warmhearted encouragement and financial support.

List of Publications

Chapter 1

"Effect of metal ion substitution on the catalytic activity of a pentanuclear metal complex"
Takuya Akai, Mio Kondo, Sze Koon Lee, Hitoshi Izu, Takafumi Enomoto, Masaya Okamura, Yutaka Saga, Shigeyuki Masaoka
Dalton Trans., **2020**, *49*, 1384.

Chapter 2

"Photochemical hydrogen production based on the HCOOH/CO_2 cycle promoted by a pentanuclear cobalt complex"
Takuya Akai, Mio Kondo, Yutaka Saga, Shigeyuki Masaoka
Chem. Commun., **2022**, *58*, 3755.

Chapter 3

"Metal Ion Substitution in a Pentanuclear Scaffold Provides an Efficient Catalyst for HCOOH/CO_2 Cycle"
Takuya Akai, Yumi Iwamura, Mio Kondo, Yutaka Saga. Shigeyuki Masaoka
Chem. Lett., accepted. DOI:10.1246/cl.230023.

Other Publications

1. "Pentanuclear iron catalysts for water oxidation: substituents provide two routes to control onset potentials"
   Vijayendran K. K. Praneeth, Mio Kondo, Masaya Okamura, **Takuya Akai**, Hitoshi Izu, Shigeyuki Masaoka
   Chem. Sci., **2019**, *10*, 4628.

2. "Dirhodium-based Supramolecular Framework Catalyst for Visible-light-driven Hydrogen Evolution"
   Pondchanok Chinapang, Hikaru Iwami, Takafumi Enomoto, **Takuya Akai**, Mio Kondo, Shigeyuki Masaoka
   Inorg. Chem., **2021**, *60*, 12634.

3. Precise manipulation of electron transfers in clustered five redox sites"
   Hitoshi Izu, Mio Kondo, Masaya Okamura, Misa Tomoda, Sze Koon Lee, **Takuya Akai**, Vijayendran K. K. Praneeth, Mari Kanaike, Satoshi Kawata, Shigeyuki Masaoka
   ChemRxiv Preprint, DOI: 10.33774/chemrxiv-2021-njtl.

4. "A Catalytic Alkylation of Ketones via sp^3 C-H Bond Activation"
   Xue Peng, Yuki Hirao, Shunsuke Yabu, Hirofumi Sato, Masahiro Higashi, **Takuya Akai**, Shigeyuki Masaoka, Harunobu Mitsunuma, Motomu Kanai
   J. Org. Chem., **2022**, DOI: 10.1021/acs.joc.2c00603